VISUALIZATION OF NODES, ANTINODES AND LATERAL DISPLACEMENTS IN VIBRATING PLATES

by

Robert D. Niven

B. Sc., University of Alberta, 1964

A Thesis Submitted in Partial Fulfillment of the

Requirements for the Degree of

Master of Applied Science

In the Department

of

Mechanical Engineering

We accept this thesis as conforming to

the required standard

THE UNIVERSITY OF BRITISH COLUMBIA

April, 1967

In presenting this thesis in partial fulfilment of the requirements for an advanced degree at the University of British Columbia, I agree that the Library shall make it freely available for reference and study. I further agree that permission for extensive copying of this thesis for scholarly purposes may be granted by the Head of my Department or by his representatives. It is understood that copying or publication of this thesis for financial gain shall not be allowed without my written permission.

Department of Mech. Eng.

The University of British Columbia
Vancouver 8, Canada

Date May 10/67

ABSTRACT

The use of optical techniques for the study of vibrating surfaces has thus far been limited to measuring small amplitudes on the order of a few hundred microinches. To extend the measuring range to much larger amplitudes a completely new technique is sought. In this thesis optical vibration methods are presented that allow amplitudes of .001" and up to be investigated, the upper limit being determined solely by the prohibitive size and cost of the equipment. The study is based on a combination of the shadow moiré deflection measuring method and the Salet-Ikeda slope measuring method which, as far as the author knows, have been applied only to the study of static situations. It is shown how these two methods may be applied to the dynamic case to permit the direct visualization of nodal and antinodal locations and displacements in vibrating plates. Three specimens are studied: a cantilever beam, a square cantilever plate and a circular free plate. Complete photographic results along with theoretical or experimental solutions are given for each specimen.

ACKNOWLEDGEMENT

I wish to express my sincere gratitude to my advisor Dr. C.R. Hazell for his generous assistance and guidance throughout the investigation and to Dr. J.P. Duncan who introduced me to the Salet-Ikeda technique and provided me with many helpful suggestions. I would also like to thank Mr. Phil Hurren and Mr. John Hoar for their valuable technical assistance.

This study was made possible through research grant No. A-3331 provided by the National Research Council of Canada.

TABLE OF CONTENTS

LIST OF FIGURES

FIGURE PAGE

NOMENCLATURE

SYMBOL

a	=	length of a side of a square plate or diameter of a circular plate
f	=	frequency.
h	=	increment of deflection on the plate surface occurring between two adjacent fringes.
p	=	pitch, centre to centre distance of either two opaque or two transparent lines on the master grid.
r	=	perpendicular distance from the optical axis to some particular line or point on a target.
t	=	plate thickness.
w	=	total deflection of plate surface measured from undeformed plane.
w_a	=	total air gap thickness between master grid and plate surface.
D	=	plate stiffness $= \dfrac{Et^3}{12(1-\nu^2)}$
E	=	modulus of elasticity.
F	=	focal length of lens.
I	=	moment of inertia
N	=	fringe order.
θ	=	slope at a particular point on plate surface.
μ	=	mass/unit length.
ν	=	Poisson's ratio

SYMBOL

ρ = mass/unit volume.

All units are in the in. - lb. - sec. system. The abbreviation lpi means lines per inch.

CHAPTER I

THE PROBLEM DEFINED

I. INTRODUCTION

In the analysis of many complex vibration problems it soon becomes obvious that solution by means of a mathemetical model is an exceedingly complicated, if not impossible, undertaking. Experimental techniques and instruments have thus evolved for the measurment of every possible type of vibration from ship's engines to the minute flutter of a diaphragm. The majority of techniques, while extremely diversified, share two things in common: (1) the readings are representative of only one point in the field, usually the point of attachment of the transducer and; (2) the measuring device must be physically placed in contact with the component under study. A difficulty of interpretation arises with the former method. In order to get an idea of the full field of vibration, numerous readings must be taken and subsequently plotted. There also exists the possibility that a point of severe vibration might be overlooked. The necessity for connecting the vibration recorder to the specimen may or may not present a problem depending on the particular component. If, for instance, a strain gauge is attached to a small thin diaphragm the increased mass and stiffness offered by the gauge may shift the response sufficiently to cause misleading results.

The appearance of the quartz crystal in the early 1920's

marked an increased interest in the field-study of vibrations. Because of the very small amplitudes involved and the shortcomings of existing measuring methods at that time, a new technique was sought. This led to the introduction of interferometric measurements which are still used and being improved upon today. Their usefulness, however, is limited to recording amplitudes in the range of a few hundred micro-inches. Since many engineering applications require a measurement of much greater values, there remains the necessity for investigating new field-measuring techniques.

In the last twenty years a variety of applications of optical principles have appeared that allow relatively large static amplitudes to be studied. However, as far as the author knows, with the exception of one very recent case none of these have been applied to the study of vibrations. Since most of them are not subject to the disadvantages outlined previously, the feasibility of applying these optical methods to dynamic situations would seem the next logical step in vibration analysis.

It was to this end that this investigation was undertaken.

II. STATEMENT OF THE PROBLEM

It was the purpose of this study to (1) develop a technique for the visualization of nodes and antinodes in vibrating plates and (2) determine, by means of stroboscopy, the deflection at any point in the plates. The study was based on existing moiré and specialized optical techniques which have thus far been used only to study plates under static loading.

III. REVIEW OF THE LITERATURE

Vibration Studies

The first experimental investigation of vibration in plates can probably be attributed to Chladni (1) in 1787. By using a fine sprinkling of sand spread over the surface of a vibrating plate he was able to observe nodal patterns for various modes of vibration. The principle involved was simply that at every point, except at the nodes, there was some finite amplitude and consequently the sand was kept in constant motion until it came to rest at a node. This technique has been applied widely in determining every conceivable nodal pattern in plates and membranes. Mary Waller (2) has made a notable contribution in this field.

A method for outlining the antinodes was discovered in the early 1800's by Savart (3). He found that a very fine powder, such as lycopodium, would tend to accumulate at the antinodes rather than the nodes. This phenomenon was later described by Faraday (4) and at-

tributed to the flow of surrounding air currents.

In the field of optical vibration analysis numerous methods have evolved which are described by Wood (5). One of primary interest was performed by Dye (6) in which he used stroboscopic interferometry to depict the surface of a vibrating quartz crystal. The technique, using a Michelson interferometer, required that a beam of monochromatic light be passed through a glass plate onto the crystal surface. The interference between the reflected beams from the two surfaces resulted in fringes representing contours of air gap thickness. When the crystal was excited the fringes rapidly oscillated over the surface causing a blur. However, by using interrupted light from a stroboscope the motion could be frozen and the fringes observed at any position. Although nodes and antinodes were not indicated directly they were easily located by proper interpretation. The method was extremely sensitive to small deflections on the order of .00005" per fringe but was too sensitive for large deflections.

A similar technique but not requiring the use of a stroboscope was presented by Osterberg (7) in 1931. Instead of freezing the motion of the fringes he developed a relationship between the intensity of the washed out fringe pattern and the amplitude of vibration. In this manner he produced patterns which readily located the nodes, and through interpretation, the antinodes. However, vibrations with amplitudes in excess of one fringe resulted in poor contrast and unsatis-

factory patterns. A multiple beam analog of Osterberg's method yielding much better results was given in 1955 by Thornton and Kelly (8).

A far more recent vibration study using holography was employed by Powell and Stetson (9). The technique requires that a continuous wave gas laser having highly coherent and monochromatic light be used as the light source. The pencil of emergent light from the laser was first split and expanded such that one beam fell on the surface of the vibration model and the other, the reference beam, was mirrored onto a photographic plate. Thus, a hologram for the time average of the coherent wavefronts scattered from the vibrating model was formed. The image reconstructed by the hologram was found to contain a system of interference fringes which were contours of constant vibration amplitude. This method allows vibrating objects with arbitrary surfaces to be analized.

The use of stereo photography has recently been applied to vibration analysis by Wasil, Merchant and Del Vecchio (10). Two identical cameras are set up so that their optical axes are parallel and slightly separated. They are then focused on a vibrating plate and simultaneous photographs taken, the motion being frozen by a stroboscope. The exposed negatives are then analyzed in a steroscope with a resulting three dimensional effect. Interpretation is somewhat complicated and requires that deflection contours be plotted.

The very latest advance in the field, and certainly the most

factory patterns. A multiple beam analog of Osterberg's method yielding much better results was given in 1955 by Thornton and Kelly (8).

A far more recent vibrations study using interferometry was employed by Powell and Stetson (9). The technique requires that a continuous wave gas laser having highly coherent and monochromatic light be used as the light source. The pencil of emergent light from the laser is first split and diffused such that one beam falls on the surface of the vibration model and the other, the reference beam, is mirrored onto a photographic plate. At the model surface the light is scattered such that a certain quanta also strike the photographic plate. The resulting intereference between the reference beam and the scattered light yields a hologram. If the hologram is now illuminated an image of the interference fringes will appear. These fringes are seen to map out contours of constant deflection.

The use of stereo photography has recently been applied to vibration analysis by Wasil, Merchant and Del Vecchio (10). Two identical cameras are set up so that their optical axes are parallel and slightly separated. They are then focused on a vibrating plate and simultaneous photographs taken, the motion being frozen by a stroboscope. The exposed negatives are then analyzed in a stereoscope with a resulting three dimensional effect. Interpretation is somewhat complicated and requires that deflection contours be plotted.

The very latest advance in the field, and certainly the most

closely related to this study, has been presented in a paper by Nickola (11). His prime interest is the dynamic response of thin membranes but the principle involved applies equally well to plates. Using the Ligtenberg moiré method, to be described later, he has succeeded in recording the dynamic partial slopes present in a membrane at resonance. In a like manner he records its transient response when struck by an impact load. In this case high speed photography is required.

Static Optical Techniques

The first part of this investigation deals with the direct determination of nodes and antinodes by using some of the more recently developed optical techniques. At present these techniques are being used solely for static analysis and it is proposed to apply them directly to the dynamic case. As will be shown later nodes and antinodes are described in terms of deflections and slopes. Therefore, with this in mind an investigation of most of the existing deflection and slope measuring optical techniques was undertaken.

It was originally believed that moiré pattern techniques would yield the best results and consequently this field was investigated thoroughly. Theocaris (12) gives a brief summary of some 85 papers written on the subject. An even more complete reference, including 173 papers, is given in a bibliography by Duncan (13).

Of the available moiré methods, three for the measurement of deflection and three for the measurement of slope, were felt to be

applicable to this study. The deflection techniques will be considered first.

Shadow Moiré

This method, although briefly mentioned by Weller and Shepard (14) as a possible deflection measuring device, saw little practical application until quite recently. Theocaris (15 and 16) shows how the shadow moiré is applied as a stepping stone in the solution of stresses in plates. The method requires that collimated light pass through a reference grid (100 - 500 lpi) onto a specimen and in so doing casts a shadow of the grid lines. By then viewing the specimen through the reference grid at an angle different from the angle of incidence of the collimated light a family of fringes will be observed, the number being proportional to the deflection at that point. The sensitivity is on the order of .005"/fringe for a 500 lpi grid. This technique will be detailed in the next chapter.

Reflection Moiré

Much like the previous method, this technique involves the viewing of a specimen through a reference grid of approximately 100 - 500 lpi. However, in this case, the specimen is polished such that the eye sees the virtual image, rather than the shadow, of the grid. The mechanical interference between the reflection of the reference grid and the grid itself yields moiré fringes proportional to the deflec-

tion. The sensitivity is approximately twice that of the shadow moiré method. This technique is presented in a paper by Ebbeni (17).

Reflection Moiré Using Diffraction Through A Fine Grid

Although it is not intended to use diffraction phenomena for this study it is included in the review because of its merit and possible future use. Introduced and developed by Middleton (18) the method is based upon the phase disturbances undergone by a beam of collimated light passing through a transparent diffraction grating and being reflected back through the grating by the surface being surveyed. The resulting fringes due to the phase interference of the component beams comprising the emergent beam indicate equal increments in air gap thickness. Sensitivity ranges between .00005" to .010"/fringe.

The following techniques are for the measurement of slope.

Ligtenberg (19)

Since its innovation this method has probably become one of the most popular, and numerous papers have been written on its various applications and refinements. Basically it involves photographing a relatively coarse grid, for example 1/16" pitch, seen reflected in the suface of the specimen. The grid is placed in the plane of the camera lens. Exposures are made of the deformed and undeformed surface using the same negative, with the result that moiré fringes of constant slope appear when the negative is developed. It has the advantage that

surface discontinuities do not show up because of cancellation in the superposition. However, for the purpose of this study it offers the problem that before photographic manipulation, fringes are not visible to the eye.

Reflection

Attributed to Theocaris (20) this method involves the use of two separate lined grids which may or may not be of the same pitch. Collimated light is passed through a master grid and is reflected from the polished surface of the specimen, through a condensing lens, onto a ground glass screen. Another grid is then affixed to the screen and by shifting it to a suitable position on the optical axis a moiré pattern will appear. If the specimen is now loaded a new pattern will become visible which, upon subtraction of the initial pattern, yields lines of constant slope. Another possibility exists, initially if the ground glass screen is perfectly aligned, the image of the master grid and the superimposed grid can be made to coincide exactly thus yielding no fringes at all. Upon now loading the specimen, lines of constant slope will appear directly without the need of subtracting the original pattern. The slopes recorded are partial slopes in a direction normal to the grid lines. Orthogonal slopes may be measured by rotating both grids through 90 degrees.

Refraction

Although quite similar to the above method this system, sug-

gested by Theocaris and Koutsabessis (21), involves the use of a transparent specimen and depends upon the refraction, not the reflection, of light. A collimated monochromatic beam is passed through a master grid, through the specimen and then imaged on a ground glass screen. All lie on the same optical axis. As before, another grid is placed on the screen and by proper adjustment a suitable moiré pattern can be formed. Loading the specimen yields constant slope lines in a direction normal to the grid lines.

Salet-Ikeda

The above methods have all depended upon the moiré phenomenon, but these are not the only, nor are they necessarily the best methods. Sabin (22), in an evaluation of numerous optical techniques offers several systems worthy of merit. One that is of prime interest is the Salet-Ikeda slope measuring technique which has been used extensively by Duncan and Brown (23) for the determination of stresses in plates. A coarse lined target on the order of 10 lpi is located at the focus of a lens. A sheet of ground glass is placed behind the target and is illuminated by a high intensity light source. The diffused light passes through the lens onto the specimen which then reflects it to another receiving lens. A pinhole just large enough to provide sufficient intensity of illumination is placed at the focal point of this lens. For a perfectly flat surface the initial observed pattern will be completely black or completely white depending on the exact position of the pinhole and type of

target grid used. The partial slopes recorded are in a direction normal to the target lines. A more complete description of this method is given in the following chapter.

IV. LIMITATIONS OF THE STUDY

The investigation is limited to the study of flat or nearly flat surfaces. The vibration is steady state in which only standing waves exist.

V. DEFINITIONS

A node is a point, line or surface in a standing wave where some characteristic of the wave field has zero amplitude.

An antinode is a point, line or surface in a standing wave where some characteristic of the wave field has maximum amplitude.

or

An antinode is a point, line or surface in a standing wave where some characteristic of the wave field has zero slope in every direction.

CHAPTER II

THEORETICAL CONSIDERATIONS

I. EVALUATION OF EXISTING TECHNIQUES

Several techniques have been presented for the measurement of deflection and slope. Since all of these are subject to various shortcomings it was necessary to evaluate them individually and in so doing choose the two (i.e. one for deflection measurement and one for slope measurement) most suitable for this study. This was done mostly by considering practical limitations of the systems.

Deflection

Three techniques were deemed to be feasible for measuring dynamic displacements. The diffraction technique, however, was not considered to be suitable for the study because of its extreme sensitivity and various complexities. The shadow and reflection moiré methods both were set up in the laboratory and their individual merits assessed. The shadow moiré was observed to give bright, high contrast patterns with specimens of light surface finish and it was found that the grid could be moved up to 3" away from the specimens before the fringes became indistinguishable. With dark surface finishes the contrast was considerably reduced. With the reflection moiré the contrast was found to be poor unless a white illuminated screen was provided as a background. In a like manner it was possible to move the grid about 3" from the specimen without losing fringe clarity. The surface finish in this case

had to be reflective. After some deliberation it was felt that the shadow moiré would be the better of the two techniques and was hence chosen for visualizing nodes and dynamic displacements. Two other factors also aided in this decision. One was the fact that the shadow moiré theory was more straight forward and did not involve the numerous approximations associated with the reflection moiré. It was also easier to use stroboscopy to stop the fringe motion since a more intense light field could be achieved. Its major disadvantage was that its sensitivity was only half that of the reflection system.

Slope

It has been shown that four suitable techniques exist for measuring slopes. The refraction moiré method was immediately disregarded since it required that special translucent models be made, which in itself was a drawback to which the other techniques were not subjected. The Ligtenberg moiré method in its original form was also rejected since fringes could not be observed before the grid lines were superimposed. This could have been overcome by inserting a sheet of glass in front of the plate specimen thereby creating a visible moiré pattern but because of the large physical size of the components in the Ligtenberg method the idea was abandoned. The main reason for this is that it is hoped that the optical equipment used in this study may, in the future, be incorporated into a measuring instrument and therefore size becomes a major factor. The two remaining methods were set up

in the laboratory and analyzed. It was hoped that the reflection method described by Theocaris would give the desired results but this was not the case. The main problem lay in not being able to get sufficiently bright clear fringes and consequently low contrast photographs resulted. This was probably due to the limitations of the equipment used. The Salet-Ikeda method on the other hand gave sharp high contrast patterns and the optical system was found to be very easy to align. This then was chosen as the slope technique for visualizing antinodes.

II. THEORY

Shadow Moiré Deflection Method

From moiré theory it is observed that if two lined grids of unlike pitch are superimposed such that their lines are approximately parallel a network of moiré fringes will appear. The appearance of these fringes is, in fact, the common "beat" phenomenon that occurs when any two similar frequencies are added together. In this case, however, the frequencies are represented by the line densities. For example, if one grid of 100 lpi is superimposed on another grid of 101 lpi, one moiré fringe per inch will appear. Another way of stating this would be to say that for every moiré fringe that is observed there must necessarily be a difference of one pitch between the two adjacent grids. A far more detailed and mathematical explanation of the moiré fringe phenomenon may be found in many of the references given by Theocaris (12) and Duncan (13).

Moiré fringes are not always produced by superimposing two grids of unlike pitch. More commonly, in fact, both grids are of identical pitch and fringes are developed in one of two ways: (1) linear stretch and/or rotation of one grid, the other being held constant or; (2) rotation of one grid in a direction normal to the other as shown in Fig. 1 (a). In the latter of these two methods the pitch of the lower grid appears to expand because of its relative rotation and in this manner achieves the pitch difference necessary to produce fringes. Assume now

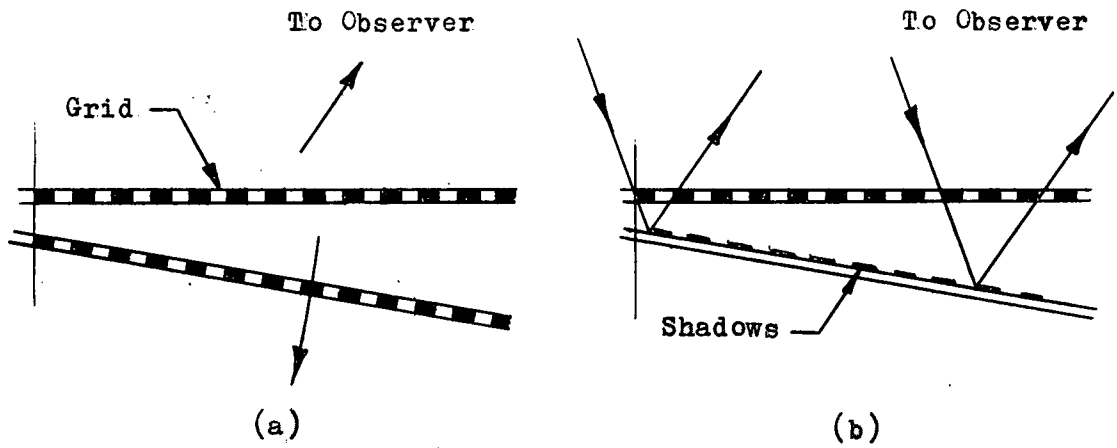

FIGURE 1

METHODS OF PRODUCING MOIRÉ FRINGES

that the lower grid is removed and in its place is substituted a plate with a matte surface. If collimated light is then passed through the upper grid, shadows will be cast on the plate surface giving the impression of a second grid. This is shown in Fig. 1 (b). When now viewed from above the interference between the master grid and the shadows is seen to yield moiré fringes. This then becomes the basis of the technique now to be discussed. Consider the system in Fig. 2.

Light source L_2 is placed at the focal point of lens L_1 in such a manner that the emergent light is collimated parallel to the AB axis. In travelling along this path the light passes through a master grid of approximately 100 to 500 lpi, thus casting a shadow of the lines on the specimen. An upper bound of 500 lpi is placed upon the grid because of the appearance of diffraction effects and low fringe contrast at higher line densities. Assume the specimen is now viewed along the axis BC and is imaged on the ground glass screen of the camera. The ground

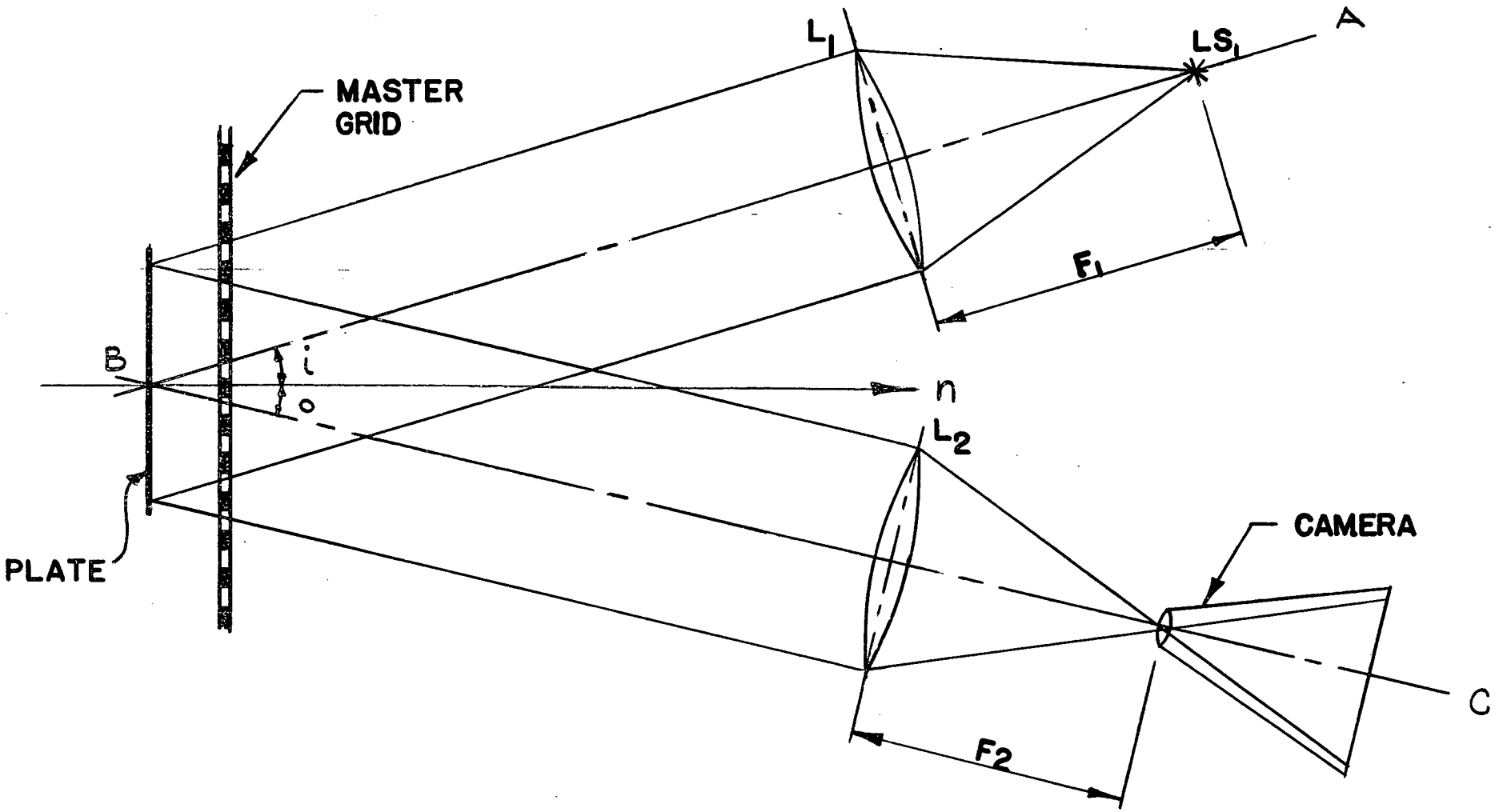

FIGURE 2

SHADOW MOIRÉ ARRANGEMENT

glass will "see" the superposition of two grids, that is, the master grid and its shadow. If initially the specimen is underformed the pitch of the shadow grid is the same as that of the master and consequently no fringes will be observed. Introduction of deformation, however, causes the apparent pitch of the shadow to change with the result that moiré fringes are generated. For the purpose of analysis it is interesting to study the deformation required to produce one fringe. Refer to Fig. 3.

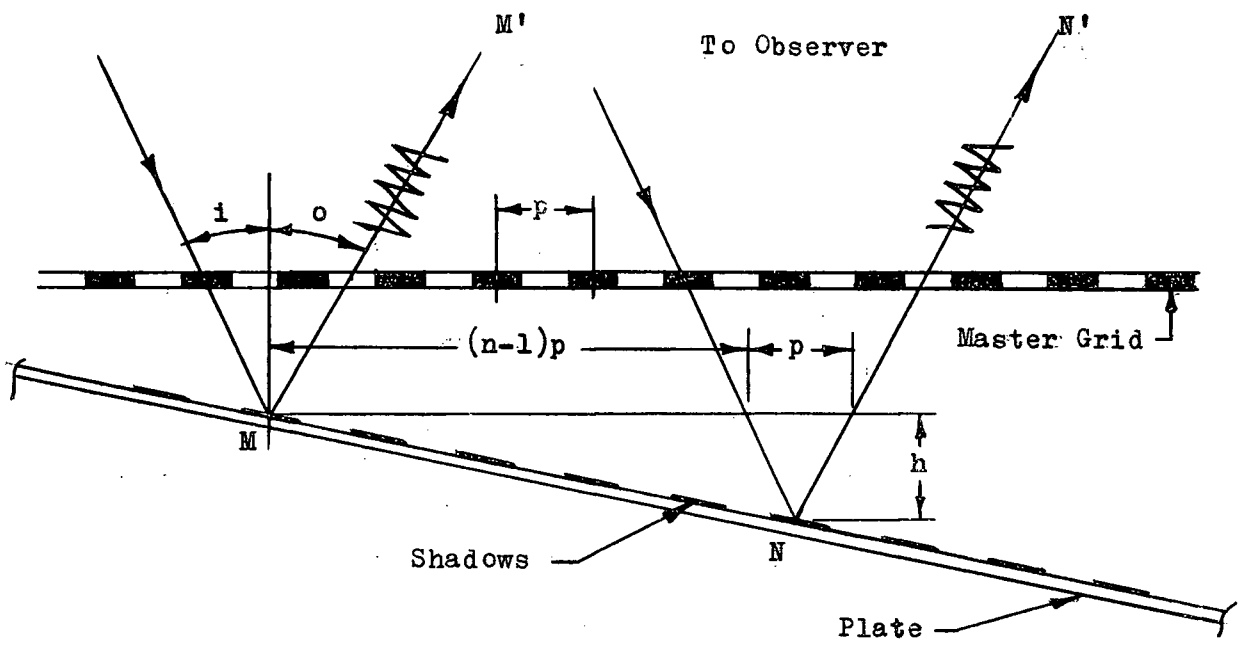

FIGURE 3

DEFLECTION CAUSING ONE FRINGE

Let the specimen be viewed along some light path parallel to the optical axis BC such that dark moiré fringes are observed along the lines MM' and NN' as shown in Fig. 3. It was previously stated that for one moiré fringe to be generated there must be a difference of one pitch between the two grids. Therefore it must be assumed that between lines MM' and NN' the number of pitches on the master grid and the number of pitches on the shadow grid must vary by one pitch. If h is the distance required to produce the mismatch of one pitch it can be seen from geometry that:

$$p = h \tan i + h \tan o$$

$$h = \frac{p}{\tan i + \tan o} \qquad (2.1)$$

or for small angles,

$$h = \frac{p}{i + o} \qquad (2.2)$$

With this information it is now possible to determine the relative deflection between any two points on the surface of the specimen. To ease interpretation it is necessary to assign each fringe a value called the fringe order N. For convenience the first fringe to appear when the plate deflects is designated the first order fringe. In analyzing a deformed plate it becomes obvious that either the dark or light fringes may be used as the reference pattern. If the objective is to determine the change in deflection between two particular points on the surface the choice of fringes is purely a matter of convenience. However, if the total deflection is required the choice of fringes becomes of the ut-

most importance. This is affected primarily by whether or not the initial unloaded field is dark or light. If the field is completely light the deflection w is given by:

$$w = Nh \qquad \text{light fringes} \qquad (2.3)$$

$$w = (N-1/2)\,h \qquad \text{dark fringes} \qquad (2.4)$$

or if the initial field is completely dark the deflection becomes:

$$w = (N-1/2)\,h \qquad \text{light fringes} \qquad (2.5)$$

$$w = Nh \qquad \text{dark fringes} \qquad (2.6)$$

Since in most cases a completely dark or light field is impossible to obtain due to deviations from flatness, it is often more convenient to cover the entire specimen with an initial fringe pattern. Such a pattern is produced by placing the plate at a slight angle to the grid and thus creating fringes "artificially". This presents the added difficulty that after deformation the initial pattern must be subtracted from the final pattern in order to determine the deflection. However, there is a distinct advantage to using this procedure, in that, a detailed analysis of the entire field is obtained. In other words, an initial "mismatch" is produced. This procedure is used frequently for the static analysis of plates loaded laterally.

In the previous discussion it is seen that each fringe order represents a particular change in height and therefore the fringe pattern is a contour map of the plate surface. Consequently the shape of the deflection curve may be found along any particular line on the surface of

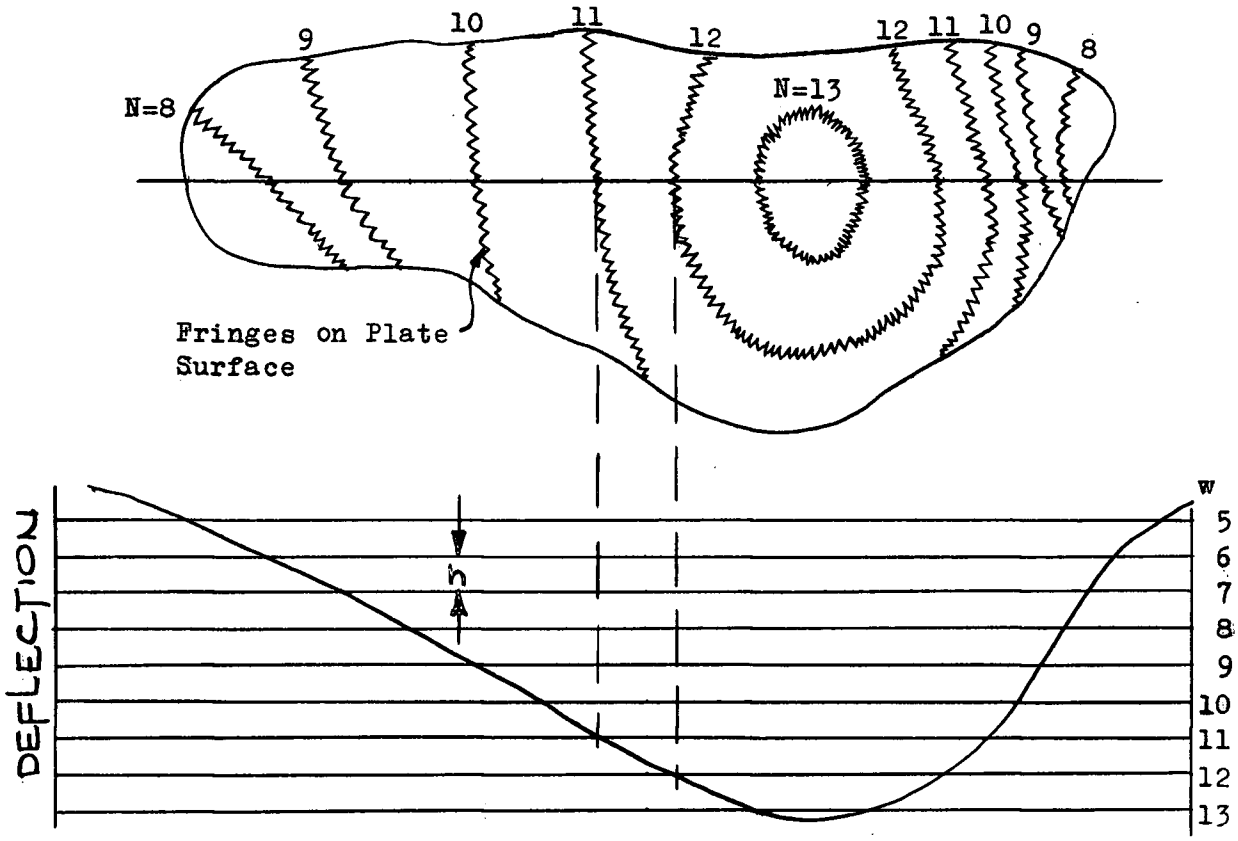

FIGURE 4

TYPICAL MOIRE PATTERN

the specimen as is shown in Fig. 4. Again the fringes may be either dark or light depending on the initial pattern used. From this diagram it is easily seen that the slope may also be evaluated anywhere along the curve by a graphical differentiation.

Salet-Ikeda Slope Method

The Salet-Ikeda technique can best be understood by considering the physical arrangement of the apparatus as shown in Fig. 5.

Consider the specimen to have a highly reflective surface and to be initially located at the intersection of the optical axes of the two

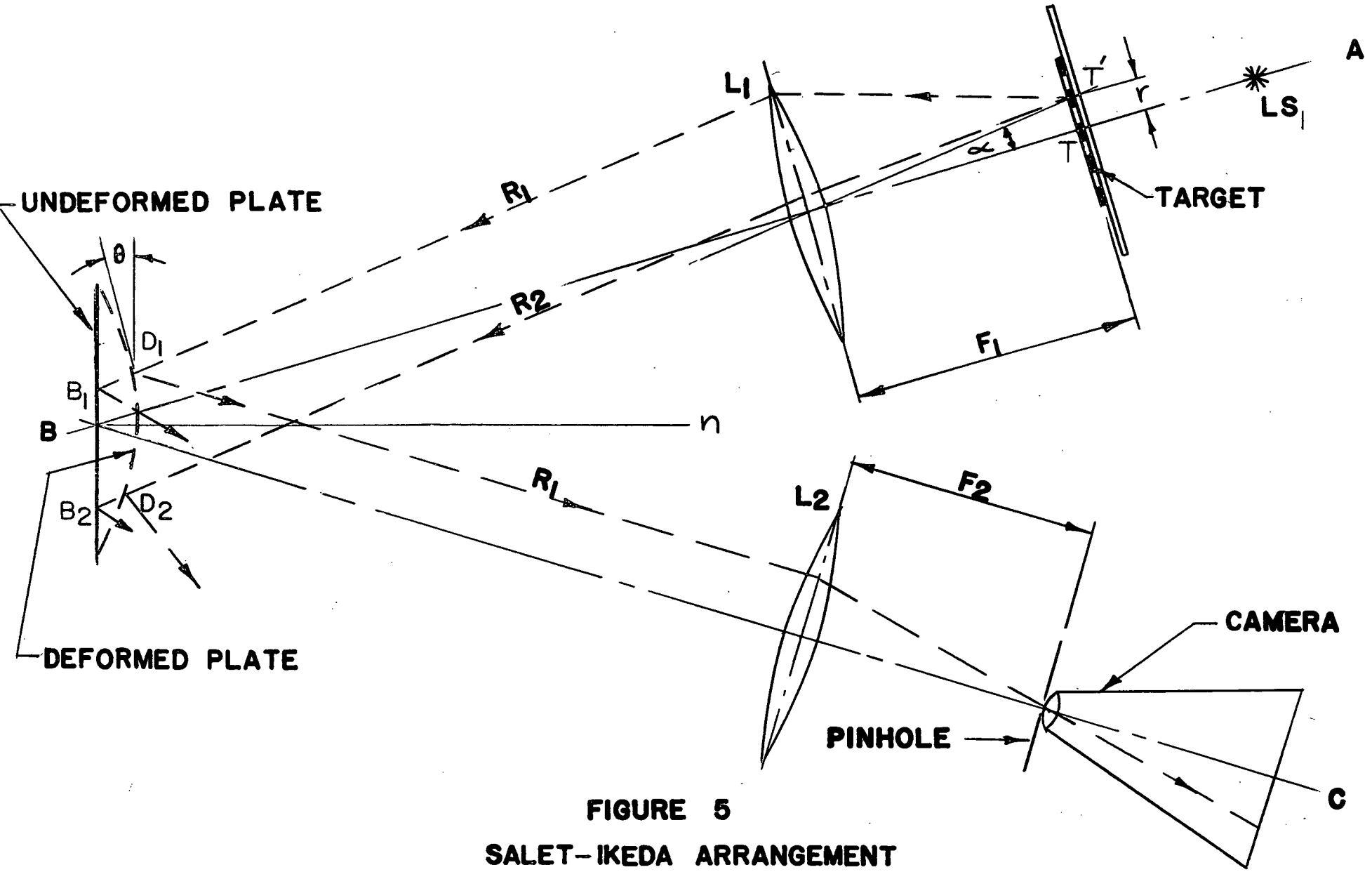

FIGURE 5

SALET-IKEDA ARRANGEMENT

lens systems. Let it be adjusted to such an angle that any light travelling along the axis AB will be reflected back along BC, through the pinhole and into the camera. A target, which may consist of straight lines, circles, dots or any suitable configuration is located in the focal plane of lens L_1 and is illuminated by a high intensity light source LS_1. Since it is desirable to have the light evenly distributed over the target surface a sheet of ground glass is mounted behind the target to act as a diffusing screen. Diffused light then passes through the target into lens L_1 where it is collimated parallel to some axis defined by its point of emission on the target. To study the effect of the deformed and undeformed plate on the paths of incident light consider two typical rays R_1 and R_2 emitted from point T' on the target. First consider the plate in the undeformed state and assume that it is perfectly flat. Since T' is not on the optical axis, R_1 and R_2 will not travel along a path parallel to the axis but rather will be inclined at an angle α. Therefore upon striking the plate at B_1 and B_2 they will be reflected off at an angle α to the BC axis and hence will not be focused at the pinhole. If, in the same manner, every single ray emitted from T' is traced through the system it will be found that they will all be reflected at an angle α and thus it is not possible in any way to observe T' at the pinhole. In fact, the only point on the target that may be observed is the point T on the optical axis. If T is a black dot or line the whole field will appear completely dark: if it is a light space the field will appear completely light.

If the specimen is now deformed the slope at every point will change with the result that the reflected rays of light will take up new paths. Again consider rays R_1 and R_2 emitted from T' on the target. Before striking the specimen at points D_1 and D_2 the rays will follow the identical path they previously took. However, because the slopes at D_1 and D_2 are now not the same the rays will be reflected in different directions. In such a manner it is possible, by varying the slope, to reflect one of the rays along some path that lies parallel to axis BC, in this case R_1. Since all the light that travels parallel to BC must be brought to focus by lens L_2 it can be seen that R_1 will pass through the pinhole and be recorded by the camera. Likewise any other point on the target which has an emergent light ray parallel to BC will also be recorded. Since the path of the emerging rays is controlled solely by the angle of rotation ϑ it is seen that this is a slope measuring method, with the lines recorded by the camera denoting contours of constant slope.

Taking r_n to be the distance between T on the optical axis and some n^{th} line on the target, and F_1 to be the focal length of lens L_1, a functional relationship is seen to exist for determining ϑ. Duncan and Brown (23) have shown the relationship to be:

$$\vartheta = 1/2 \tan^{-1} \frac{r_n}{F_1} \qquad (2.7)$$

Since ϑ is direction dependent the choice of targets and their line orientation is of the utmost importance. However, regardless of what type of target is used it should be noted that the direction

of the slope is always normal to the direction of the target lines. For example, a circular target yields contours which join points of equal slope in the radial direction.

In the previous discussion it was assumed that the plate was perfectly flat before loading. This does not limit the technique, however. If the unloaded plate has some initial curvature it will yield a very definite pattern when viewed through the pinhole. Upon loading, however, the pattern will be observed to change. If the initial pattern is then subtracted from the loaded pattern the slopes will be given directly. This is often very necessary since the technique is extremely sensitive to the slightest deviation from flatness.

Analysis of Nodes and Deflections

From the definition given in Chapter II it is seen that for a point to be a node the amplitude at that point must remain zero for all time. Therefore, any system that has the ability to scan a vibrating plate and pick out the zero deflection points would be a suitable measuring device. Since the shadow moiré method has the advantage of being able to depict the contours of deflection everywhere in a deformed surface and since no mechanical attachment to the surface is necessary it would seem to be a very desirable technique. Its feasibility for visualizing nodal patterns will now be investigated.

It has already been shown in Fig. 3 that as a plate deforms

a new moiré fringe will appear for each increment of deflection h that the plate undergoes. Therefore if the plate in Fig. 6 (a) is deliberately placed at an angle to the grid an initial fringe pattern will be created on its surface. Consider now that the plate is set into a state of resonance and assumes the mode shown in Fig. 6 (b). Nodes are indicated at A and B.

To study the motion of the fringes as the plate oscillates between its two maximum amplitudes it is first convenient to investigate one particular fringe occuring at point P. This fringe is a contour line representing the deflection w_8 and regardless of what happens to the shape of the plate this fringe is obliged to shift to any point having this deflection. Therefore as the plate deflects upward from its undeformed position 1 to some new position 2, the P fringe will migrate along the w_8 contour to P'. Similarly if the motion of every other fringe is investigated it will be observed to behave in a like manner. Thus the entire fringe field appears to sweep across the plate in the directions indicated by the arrows. At the nodes, however, the deflection is constant. Therefore fringes appearing there remain fixed. If the motion is now investigated as the plate deflects downward to position 3, the P fringe is seen to shift along the w_8 contour to P''. As in the above case the fringe field sweeps over the surface in step with the P fringe, with the exception that it is now moving in the opposite direction. Again the fringes occurring at the nodes remain stationary. Therefore, as deflection occurs the fringes either approach or leave the nodes but at no time ever cross them.

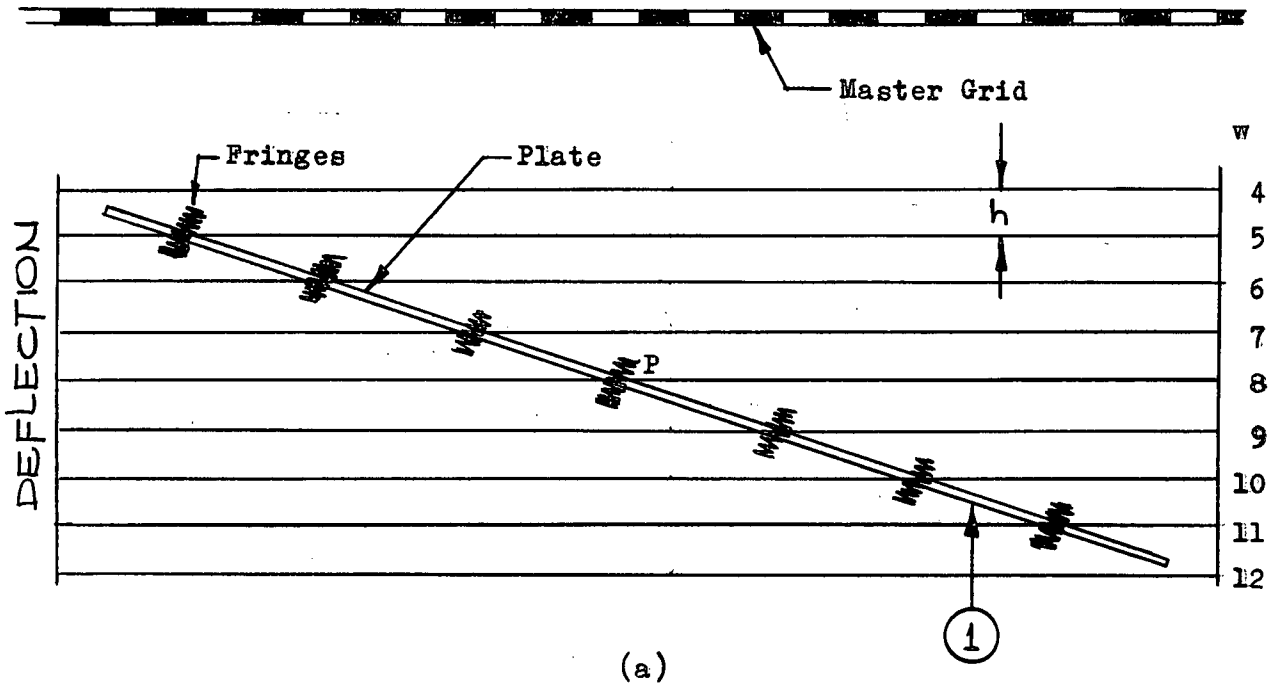

(a)

PLATE AT REST

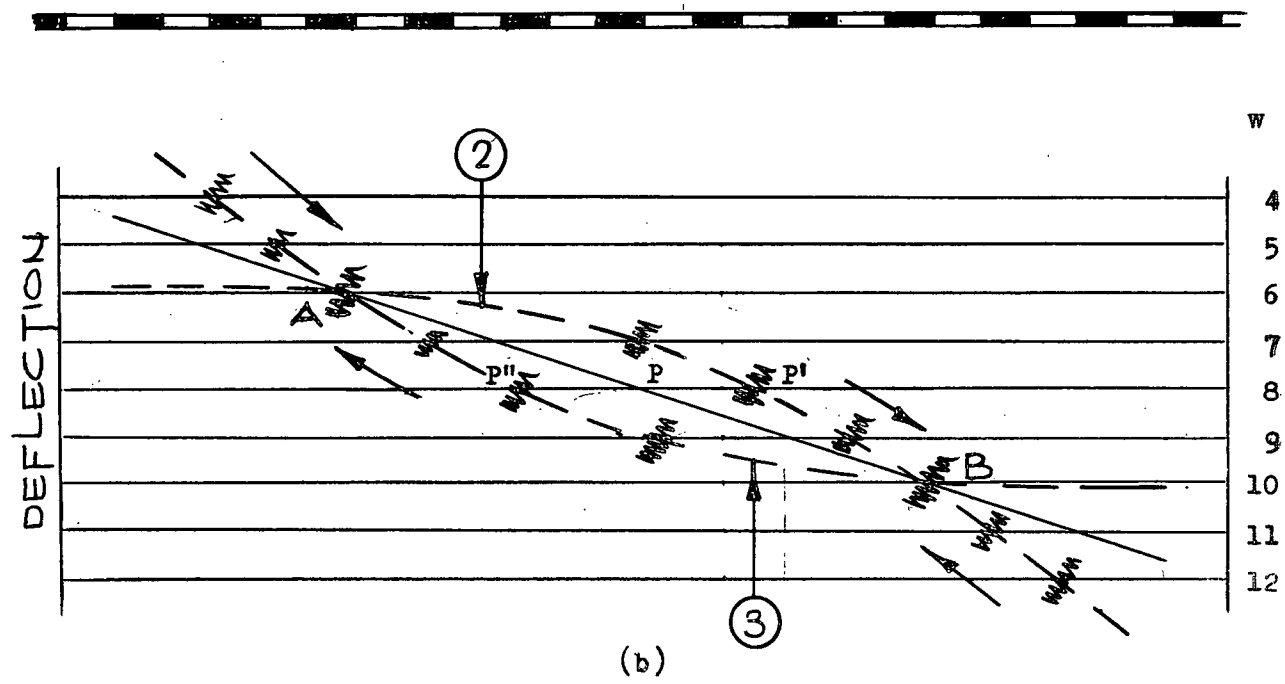

(b)

PLATE AT RESONANCE

FIGURE 6

MOIRÉ FRINGE MOTION IN A VIBRATING PLATE

During vibration the fringe sweeping action is greatly increased since the fringes are moving at a very high velocity. This rapid oscillation of the pattern results in a blurred image and is termed "washout". If the eye is used to view the vibrating pattern a lower limit is placed on the ability to observe fringe blurring. This arises out of the fact that the eye retains an image for 1/30 sec. Anything moving slower than this will not be blurred. The camera, however, is far less restricted since by using a time exposure even the slowest moving pattern will lead to washout.

The principles and facts outlined enable the nodal patterns and deflections to be observed and recorded everywhere in the plate. The pattern of the nodal lines are revealed directly as in Fig. 7 and need no further interpretation. To determine the deflections it is necessary to "stop" the motion of the fringes by either of the following techniques: (1) a stroboscope flashing at the same frequency as the plate or; (2) high speed photography. In this manner it is possible to record the fringe pattern at any particular instant and then "subtract" the indicated deflection from the static deflection to obtain the deflection due to vibration.

Up to this point nothing has been said regarding the effect of amplitude on the character of the observed nodal pattern. This factor is of major interest since it imposes both an upper and lower limit on the capacity of the technique to reveal nodes. If the amplitude of vibration is small the fringe shift on the plate surface will likewise be small.

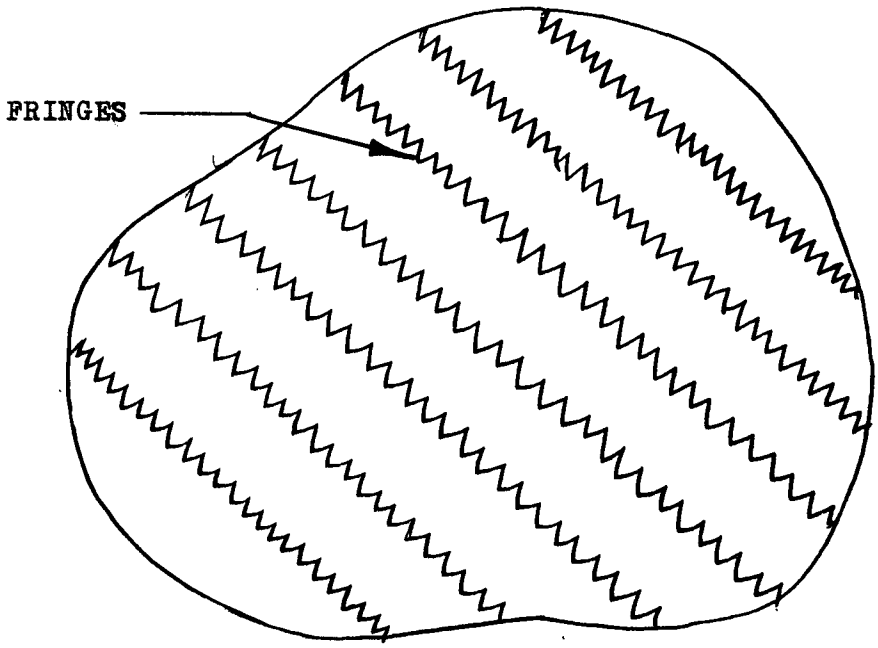

(a) STATIC PATTERN

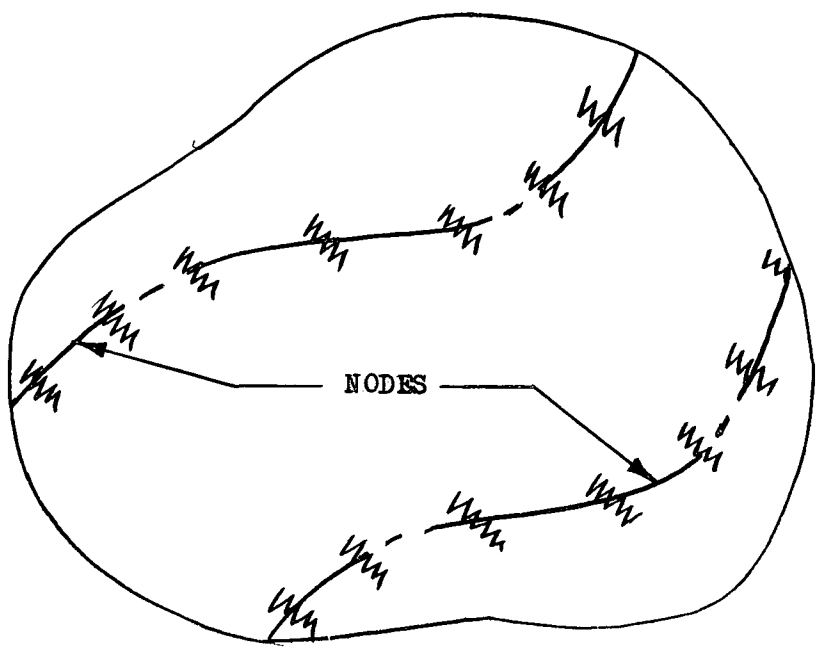

(b) DYNAMIC PATTERN

FIGURE 7

TYPICAL NODAL PATTERN

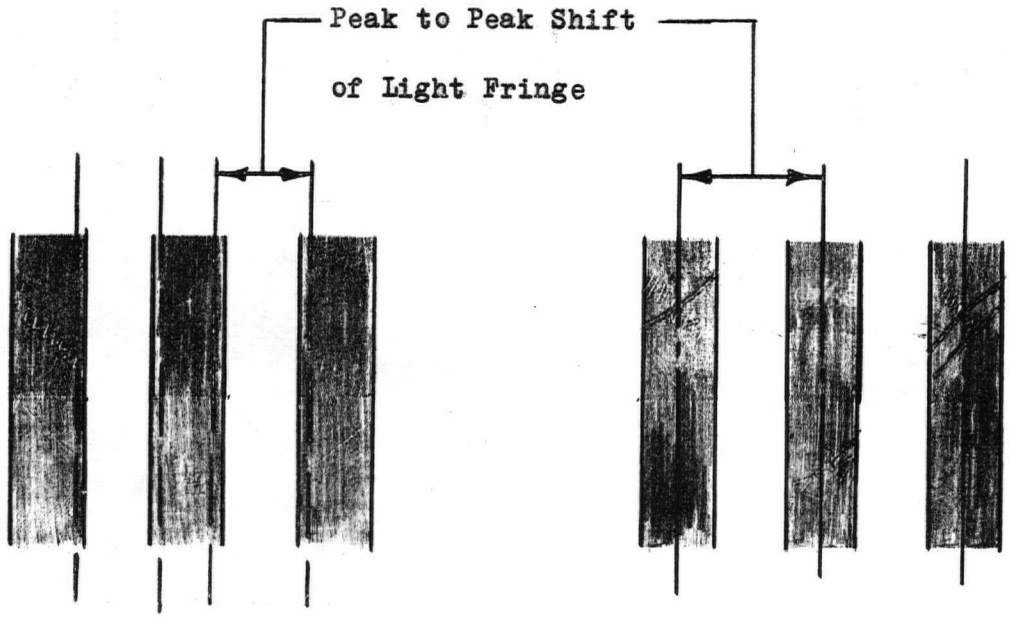

(a) DARK FRINGE NOT WASHED OUT (b) DARK FRINGE WASHED OUT

FIGURE 8

FRINGE SHIFT NECESSARY FOR WASHOUT

If the shift is on the order of 1/10 of a fringe width as shown in Fig. 8 (a)this is insufficient to washout the dark fringes and therefore ineffective in defining the node. The minimum fringe shift necessary for washout is shown in Fig. 8 (b) and is found to be 1/2 a fringe width or in terms of deflection:

$$w_{min} = \frac{h}{4} \qquad (2.8)$$

The upper bound is more difficult to evaluate. It has already been shown in Fig. 6 that the amplitude has no effect on the movement of the fringes at the node. It does, however, alter the width of the nodal band. As the amplitude is increased the node will appear to become progressively narrower until finally it reaches a point at which there

is insufficient contrast to make it clearly visible. This can only be appreciated by actually viewing the pattern while varying the amplitude.

ANALYSIS OF ANTINODES

From the second definition of an antinode given in Chapter II it is apparent that if a point is an antinode the slope of all lines passing through the point must be equal to zero. Stated mathematically this becomes:

$$\frac{\partial w}{\partial n} = 0 \qquad (2.9)$$

where n is the direction of some arbitrary line occuring at the antinode.

Although it would be most desirable to investigate perfectly flat plates this places a limitation on the analysis and therefore the plates will be assumed to have some initial warp. The perfectly flat plate will then be treated as a special case.

The Salet-Ikeda technique will now be investigated as a means of locating antinodes.

In the previous discussion of the Salet-Ikeda technique it was shown that if a deformed or warped surface was placed in the optical system, a pattern of lines would appear on the photographic screen. Each line was found to be a constant slope contour on the plate surface, the direction of the slope being measured normal to the direction of the target lines. This situation for a small element of plate is shown greatly exaggerated in Fig. 9 (a). Here the reflected rays are all para-

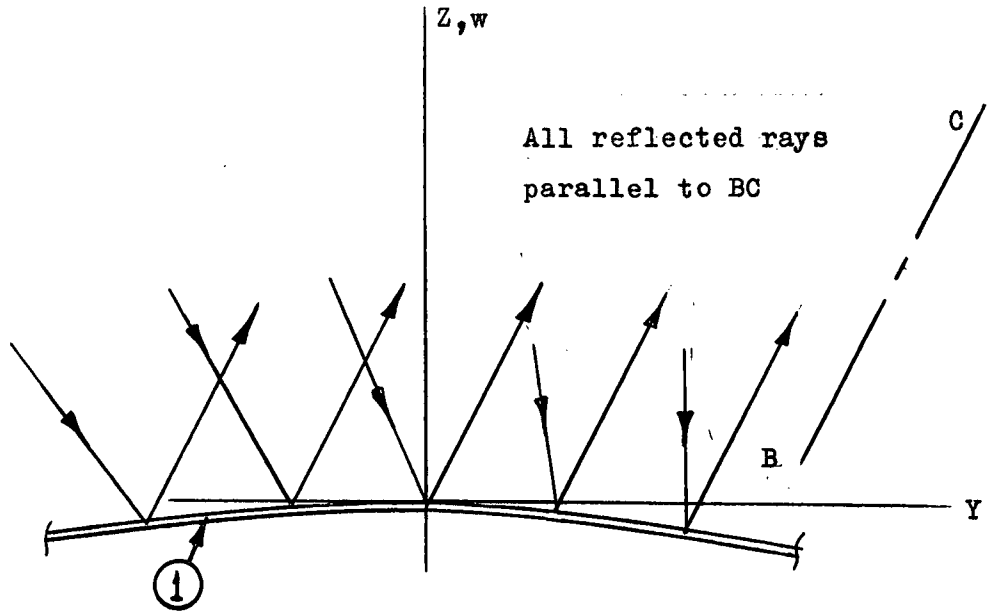

(a)

PLATE AT REST

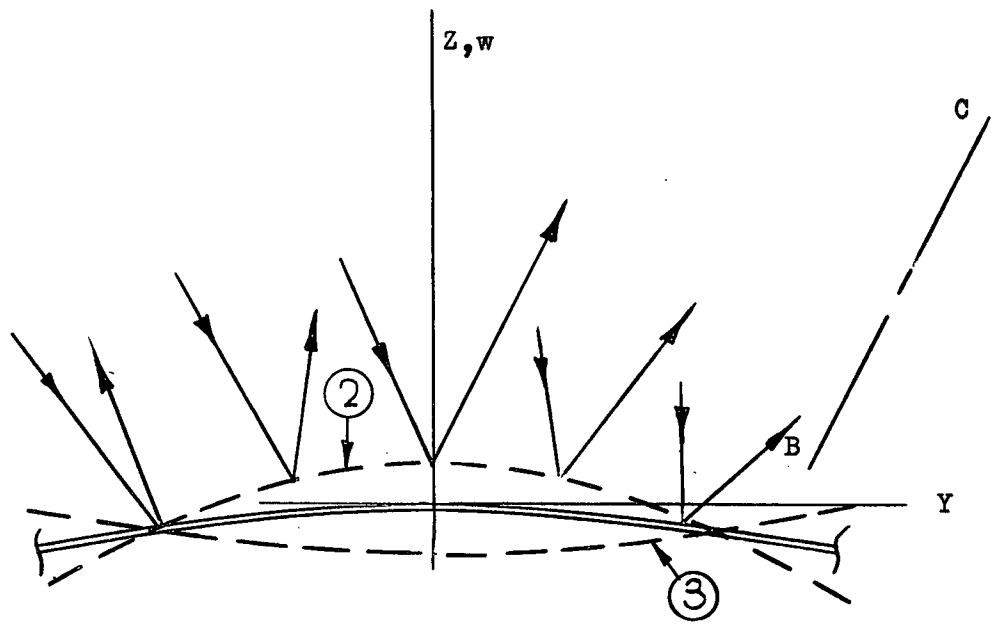

(b)

PLATE AT RESONANCE

FIGURE 9

MOTION OF LIGHT PATHS REFLECTED OFF A VIBRATING PLATE

llel to the optical axis BC and hence recorded by the camera. Let the plate now be excited at some natural frequency and assume that it takes the shape shown in Fig. 9 (b). If the plate is examined when it reaches the position 2 it will be observed that nearly every reflected ray that was initially parallel to BC is now reflected in some random direction which is not parallel to BC. In fact the only reflected ray that maintains its original direction is the one at the antinode. The same condition applies as the antinodal contour line travels to position 3. Thus as the plate oscillates rapidly between its maximum amplitudes every ray, with the exception of that at the antinode, sweeps back and forth and in so doing cannot be detected as a continuous signal at the pinhole. The antinode ray, however, appears to remain fixed with respect to the plate so that any pattern or line that occurs at that point will necessarily remain motionless.

Vibrating plates represent a condition of two dimensional wave motion and hence there exists the possibility of having two dimensional standing waves. Partial waves will be detected in particular directions, each with nodes and antinodes. The antinodes for any one particular wave oriented in the ξ direction are defined by $\frac{\partial w}{\partial \xi} = 0$ However, because this wave is interacting with waves oriented in other directions the slope in the orthogonal direction is not necessarily zero and hence the condition for an antinode given in eqn. 2.9 is not satisfied. Thus it is convenient to refer to the direction dependent antinode as a "partial antinode" in the ξ direction. If the ξ wave is continuous across the entire plate the partial antinode will likewise traverse

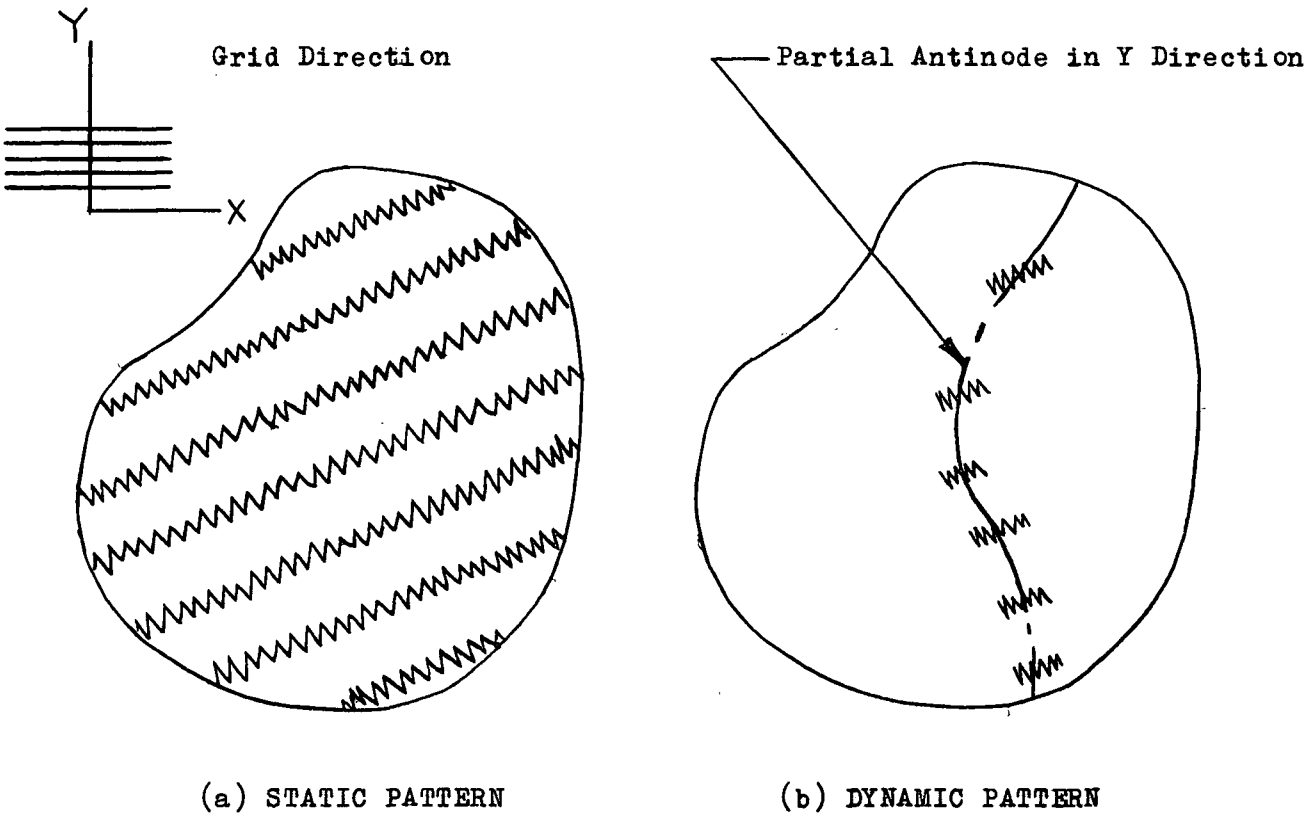

FIGURE 10

TYPICAL PARTIAL ANTINODE PATTERN

the entire plate. A typical pattern is shown in Fig. 10.

In the Salet-Ikeda technique it was just shown that antinodes may be readily detected by the fact that the pattern or line at that point does not washout when vibration is introduced. The question now arises, what kind of antinode does it measure -- the true antinode described in eqn. 2.9 or a partial antinode described in the last paragraph? Since only straight line targets are used the technique measures slopes in only one direction and thus under vibration is seen to measure partial

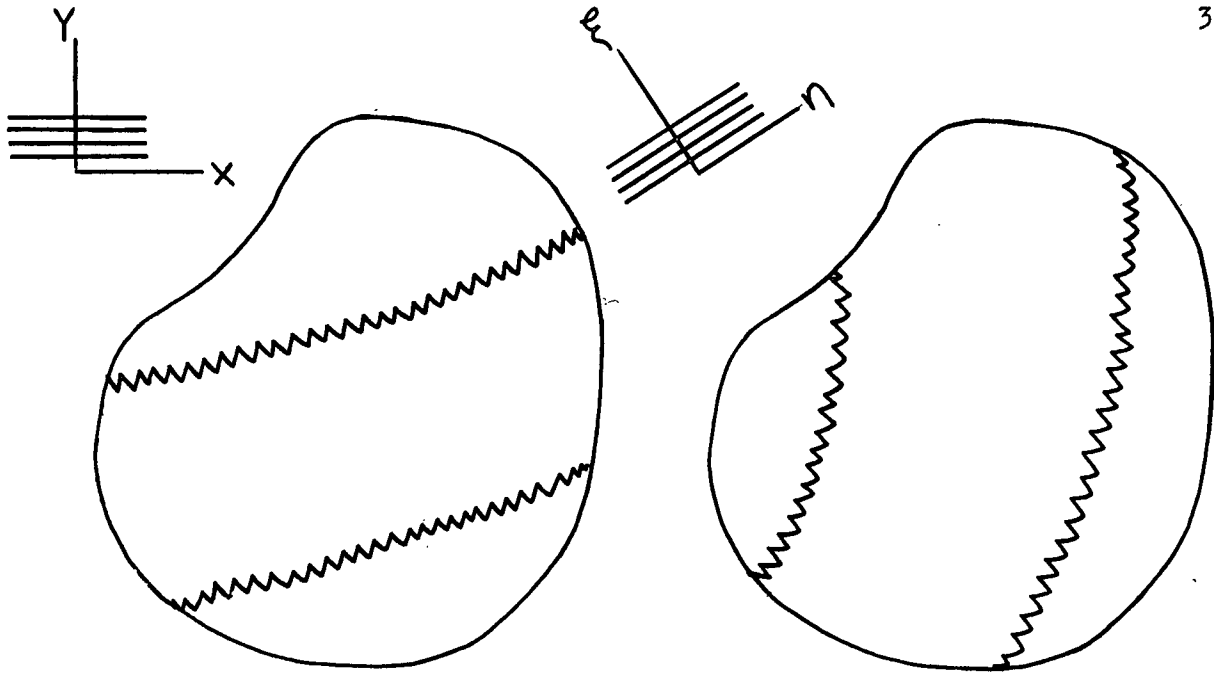

(a)

PARTIAL ANTINODE IN Y DIRECTION

(b)

PARTIAL ANTINODE IN ξ, DIRECTION

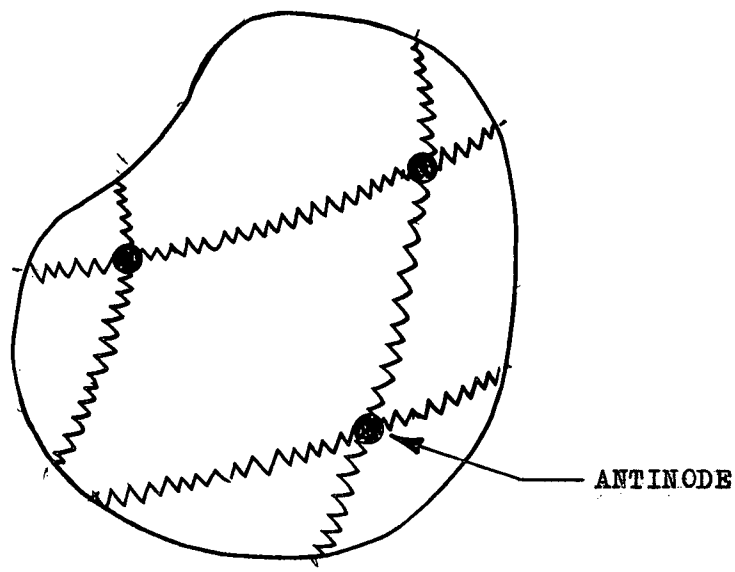

(c)

SUPERPOSITION OF PARTIAL ANTINODES

FIGURE 11

METHOD OF LOCATING ANTINODES

antinodes. It is completely insensitive to slopes in the orthogonal direction and hence cannot detect true antinodes.

Since the antinode cannot be observed directly a method for locating it must be found. An antinode by definition has zero slope in every direction and therefore it must necessarily lie on a partial antinode. Thus if two partial antinodes of different direction are superimposed the true antinode must lie at their intersection point as shown in Fig. 11.

To extend the technique to the study of perfectly flat surfaces it is only necessary to shift the pinhole along the optical axis to some point that is not at the focal point of lens L_2. In this manner the pinhole is capable of viewing a much greater area of the target and thus has the effect of creating an initial pattern on the plate surface. Although this is a departure from exact Salet-Ikeda theory it is of no importance since quantitative results are not required. If the plate is now vibrated exactly the same effect will be observed as occurred in the case of the warped plate. Another method that could be applied to flat plates would be to locate the pinhole at the focal point of lens L_2 and then by manipulating the target produce a completely dark field on the plate. Upon exciting the plate antinodes would appear directly as black lines.

In the previous analysis only straight line targets were discussed. Although the technique is not limited to the use of this type of

target alone it is found that the results are easier to interpret.

Beam And Plate Specimens To Be Studied

In the investigation three particular shapes are examined: (1) a cantilever beam; (2) a square cantilever plate and; (3) a circular free plate. Since the solution of the cantilever beam is well known and many tables relating to its characteristics have been published this is chosen as the primary specimen and is hence used in determining the exact location of the nodes and antinodes as well as the deflections. Similarly tables exist for the solution of the square and circular plates (24, 25 and 26) but as an alternate solution the nodes are determined by means of Chladni sand patterns. No solution is given for the location of the antinodes in these two plates. It is considered sufficient to show the theoretical location of the antinodes in a cantilever beam.

All the pertinent equations relating to the specimens are given in Appendix A.

Calibration Of The Cantilever Beam

In order to evaluate the shadow moiré method as a dynamic displacement measuring technique it is necessary to provide a means of comparing the obtained results with known values of displacement. The cantilever beam is considered an ideal specimen for this purpose because of its well known and simply applied solutions. If the beam is vibrated at its fundamental frequency it is found that its deflection vs

x/L curve due to inertia loading is almost identical to the curve produced by loading a similar weightless beam with a point static load applied at its free end. These curves are shown in Fig. 12. It can be seen that the maximum deviation between the curves occurs at about x/L = .5 and is roughly 3 per cent. However, very close to the fixed end the difference becomes negligible. If a strain gauge is placed as close to this end as possible it will yield approximately the same output for both the dynamic and static deflection at the free end. Since the static deflection can be easily determined it is only necessary to apply known loads to the beam and note the output of the strain gauge on some recording device. If the dynamic case is then analyzed, by comparing its strain gauge output to that of the static case the deflection may be determined directly. This, however, is for the free end only and to find the deflection at any other point the dynamic curve must be used.

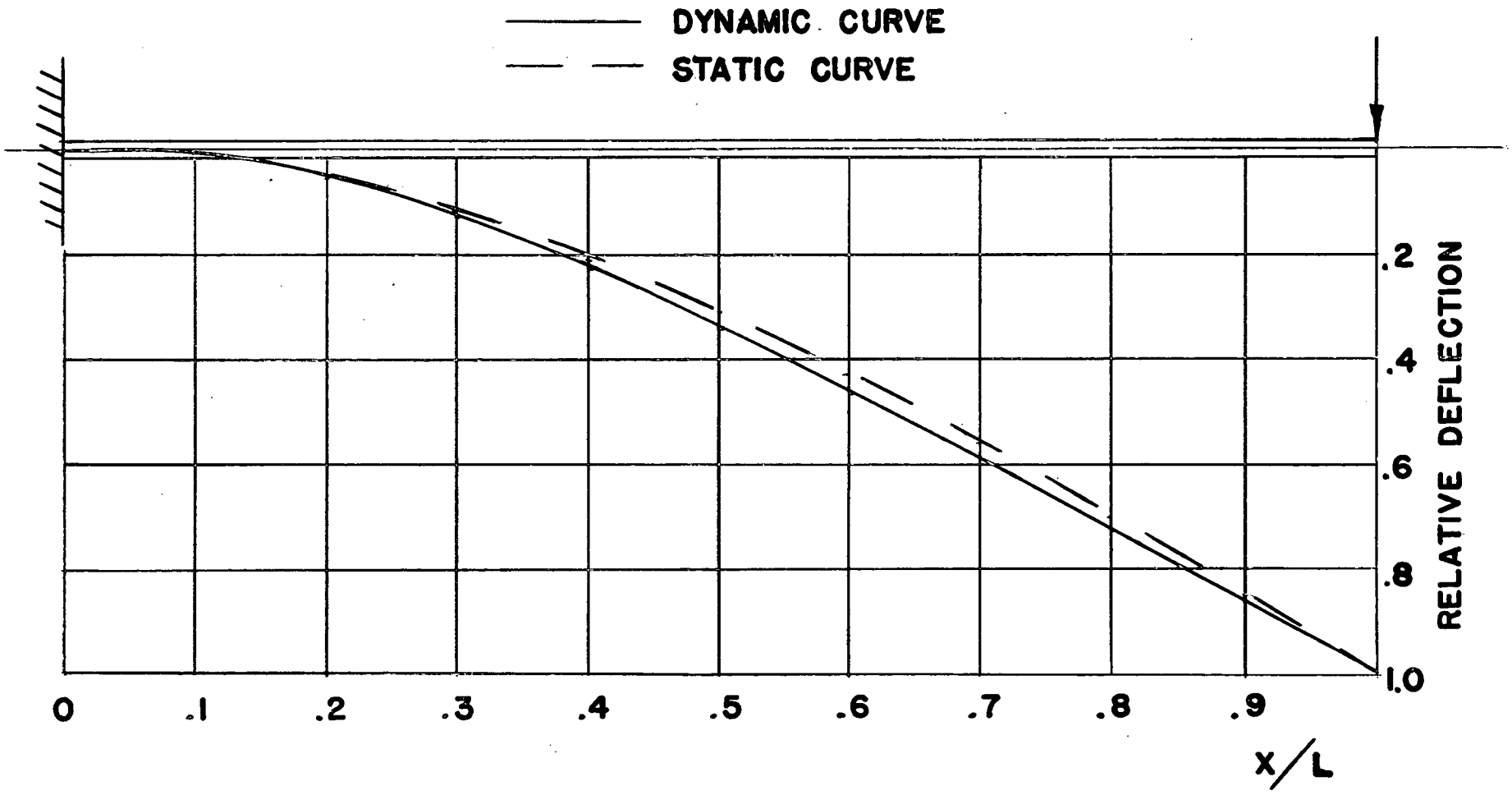

FIGURE 12
STATIC AND DYNAMIC DEFLECTION CURVES

CHAPTER III

EXPERIMENTAL APPARATUS

I. OPTICAL SYSTEMS

Shadow Moiré

The geometrical placement of the components has already been given in Fig. 2. This was somewhat of an idealized system and it was necessary and convenient to make certain modifications. The point light source, for instance, is by definition an infinitely small point of light, to which tungsten filament and mercury vapor lamps are a poor approximation. To improve this situation it was necessary to introduce a light condenser followed by an iris diaphragm as shown in Fig. 13.

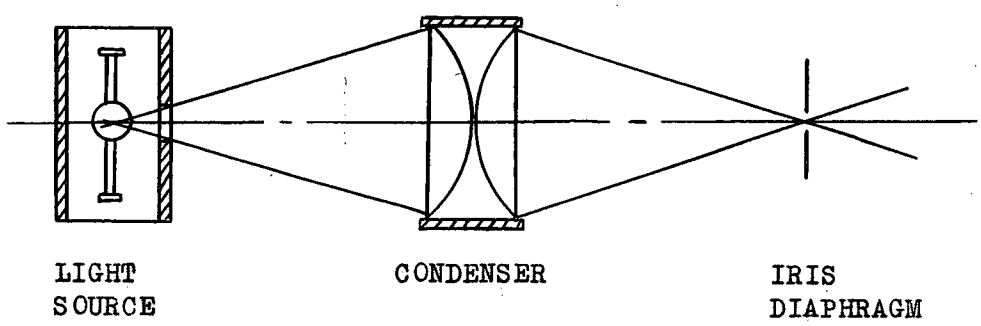

FIGURE 13

SHADOW MOIRÉ LIGHT SOURCE

The lenses used in this condenser were 5" in diameter and had a focal length of 7". The iris diaphragm had a minimum aperature of 1/16".

In order to obtain the maximum light intensity an Osram HBO 200 W/2 mercury vapor lamp was used as the light source. Because of the danger of explosion and ultra violet radiation the lamp was enclosed in a thin aluminum tube 3" in diameter by 6" long. This also acted as a draft tube and provided sufficient cooling. The light emitted by the lamp was found to contain 3 major wave lengths, green being the most prominent. For the purpose of minimizing diffraction effects at the grid all the wavelengths except green were eliminated by using a Kodak #58 (B) filter.

The power required to operate the lamp was provided by a Model P-210D power supply available from George W. Gates and Co.

All the equipment incorporated in the light source arrangement is shown in Fig. 14.

Lenses L_1 and L_2 as shown in Fig. 2 were both high quality field lenses each having focal lengths of 60". Lens L_1 was 12" in diameter, lens L_2 10" in diameter. Both were mounted in adjustable supports.

Two master grids were used in the investigation, one of 242 lpi and one of 500 lpi. Both were produced photographically from etched masters by contact printing onto 8" x 10" glass plates. To sup-

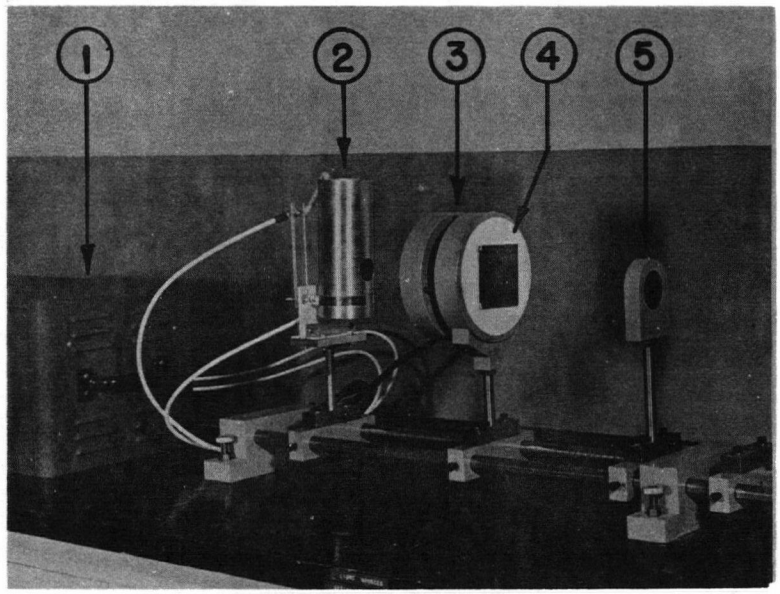

FIGURE 14

SHADOW MOIRÉ LIGHT SOURCE

LIST OF COMPONENTS

(1) power supply

(2) light source

(3) condenser

(4) filter

(5) iris diaphragm

port the grid a sturdy frame having 3 degrees of movement was constructed. The grid mounted in its frame is shown in Fig. 15.

The camera used in the study was a 4" x 5" Calumet with a 240/480 mm. Schneider lens.

The entire shadow moiré arrangement is shown in Fig. 22.

Shadow Moiré Using Stroboscopy

For the determination of dynamic deflections it was necessary to freeze the motion of the fringes. This was carried out by using a General Radio Model 1531-A stroboscope. Because of the intermittent intensity produced by this instrument the overall intensity for the purpose of taking pictures was quite low. In order to use as much light as possible the condensing lenses and iris diaphragm were dispensed with and the lamp itself was placed at the focal point of lens L_1. The stroboscope came complete with its own reflector which had to be removed. In its place was substituted a large 8" spherical mirror with a focal length of 2 1/2". The mirror was adjusted until the strobe lamp was located at its center of curvature. In this manner all the light collected by the mirror was reflected back through the source. The arrangement is shown in Fig. 16.

Salet-Ikeda Technique

If the Salet-Ikeda arrangement in Fig. 5 is compared to that of the shadow moiré in Fig. 2 it is observed that, with the exception.

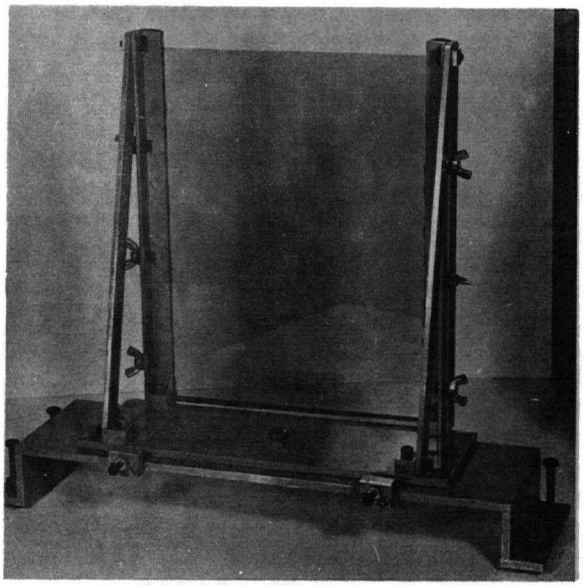

FIGURE 15

GRID AND SUPPORT FRAME

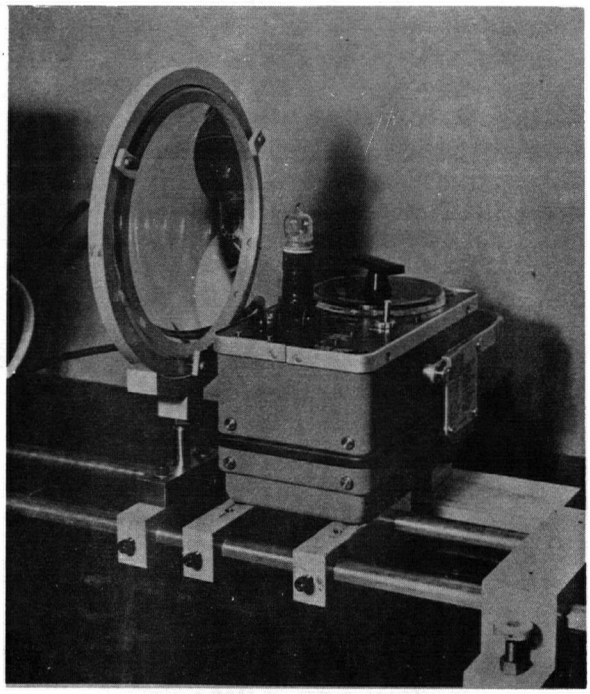

FIGURE 16

STROBOSCOPE WITH SPHERICAL MIRROR

of the target, and the pinhole in front of the camera, the two systems are identical. For this reason the same lenses and light source as were described for the shadow moiré were used for both techniques.

The Salet-Ikeda technique did not require the use of a point light source but instead required that a well illuminated target be placed in the focal plane of lens L_1. To achieve the required illumination the source and condensing system were set up as previously described. However, the iris diaphragm was removed and replaced by a sheet of ground glass. The ground glass was not placed at the focal point of the condensing lens, however, but was shifted to a point at which it was covered by a fairly uniform light field as is shown in Fig. 17.

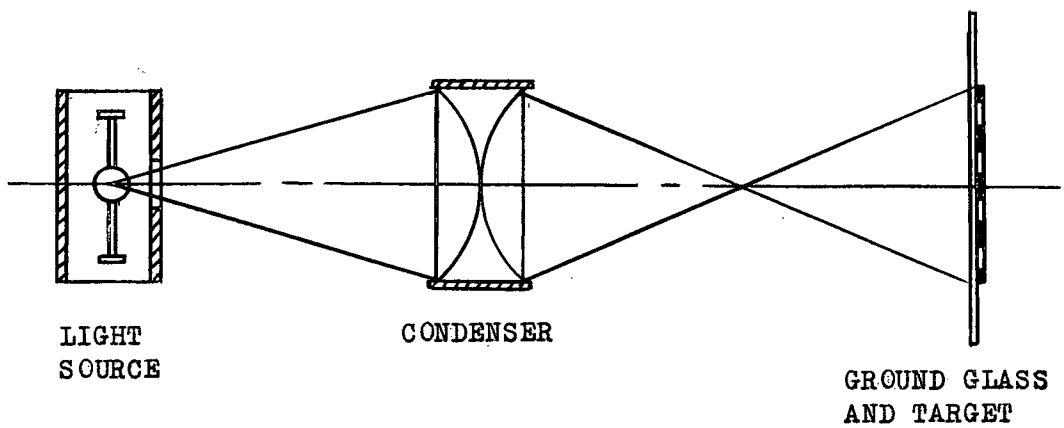

FIGURE 17

SALET-IKEDA LIGHT SOURCE

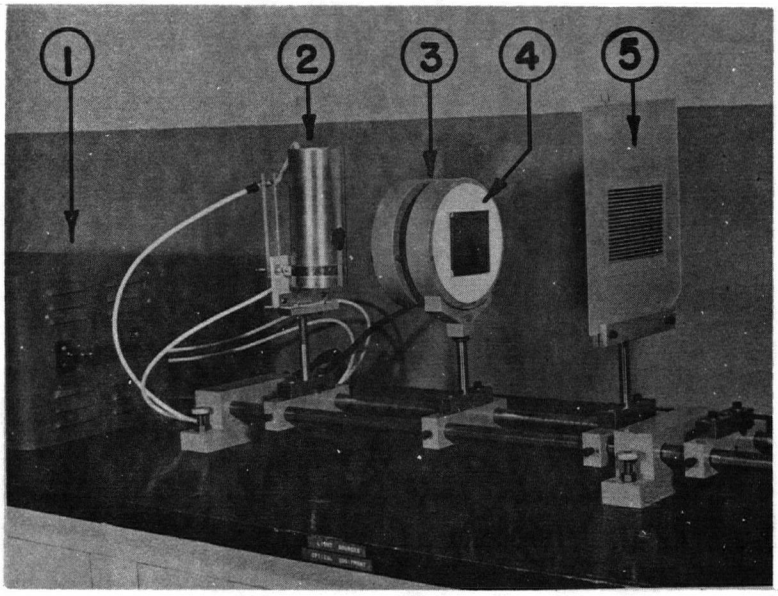

FIGURE 18

SALET-IKEDA LIGHT SOURCE

LIST OF COMPONENTS

(1) power supply

(2) light source

(3) condenser

(4) filter

(5) target

A target was then affixed to the surface of the ground glass downstream of the light source. Three main targets were used, 4 lpi, 7 lpi, and 20 lpi. These were made by drawing parallel lines on a sheet of paper and photographing them. The negative was then placed in the enlarger and by varying the degree of enlargement and exposing a sheet of high contrast film, targets of any suitable density could be made.

Pinholes of various diameters were investigated but it was found that the lowest f/stop on the camera, approximately f/60, yielded sufficient clarity of fringe image and was therefore used throughout the experiment.

The light source with target attached is shown in Fig. 18. The entire Salet-Ikeda arrangement is shown in Fig. 23.

II. VIBRATION APPARATUS

Vibration Generating Equipment

The apparatus used to set up vibration in the specimen is shown in Fig. 19. It consisted of a Goodmans V 47 - 3 Ω vibration generator attached to a solid steel base. The backing plate on which the generator was mounted was made adjustable so that contact between the specimen and the generator could be set to any suitable position. A heavy steel bar was attached to the top of the base to which the vibration specimens were clamped.

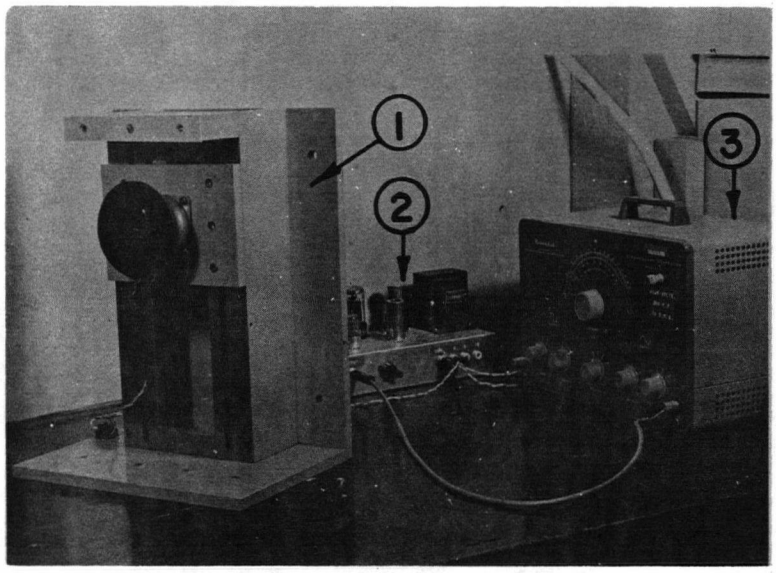

FIGURE 19

VIBRATION GENERATING EQUIPMENT

LIST OF COMPONENTS

(1) vibration generator and base

(2) amplifier

(3) audio generator

Power for the generator was supplied by a 10 watt amplifier driven by a Heathkit audio generator. Voltage and current meters were inserted in the circuit to monitor overload.

Test Specimens

Three specimens were studied:

(a) square plate - 4" x 4" x .058" thick plexiglass

(b) cantilever beam - 4" x 1/2" x .058" thick plexiglass

(c) circular plate - 4" dia. x .030" thick plexiglass

In the previous discussion it was seen that two surface finishes were required on the specimens, reflective and matte. The reflective finish was produced by painting the back surface of the specimens with a flat black paint. In a like manner, the matte surface was produced by spraying the front surface with flat white paint.

In the tests the square plate and beam were both clamped solidly to the steel base but were not rigidly connected to the vibration generator. The circular plate, however, was free on the edge and had to be supported by the generator spindle. This meant that some form of attachement had to be devised. This was done quite successfully by drilling and tapping a piece of 1/8" plexiglass to the size of the spindle screw and then grinding the edges down to a small circular disc about 3/16" in diameter. The small disc was then bonded to the centre of the plate with acrylic cement. After drying, the spindle

screw was firmly screwed into the disc and the plate securely held.

Displacement Calibration Instrumentation

The apparatus shown in Fig. 20 was used to determine the displacements induced in the vibrating cantilever beam.

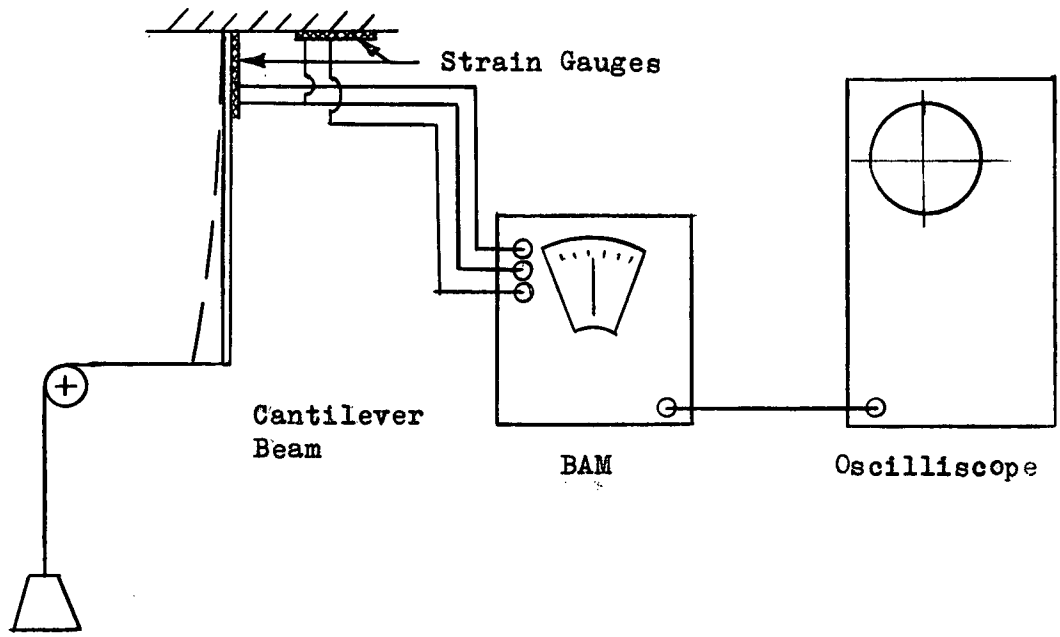

FIGURE 20

INSTRUMENTATION

Weights varying from 1/16 oz. up to 1/4 oz. were attached by means of a fine thread to the end of the cantilever. The deflection introduced by the loading was recorded by Lima-Baldwin CD-8 strain gauges, one active and one dummy. This information was then fed into a Bridge Amplifier Meter Model BAM-1 and after amplification into a Tektronix Model 502A oscilliscope. The equipment is shown in Fig. 21.

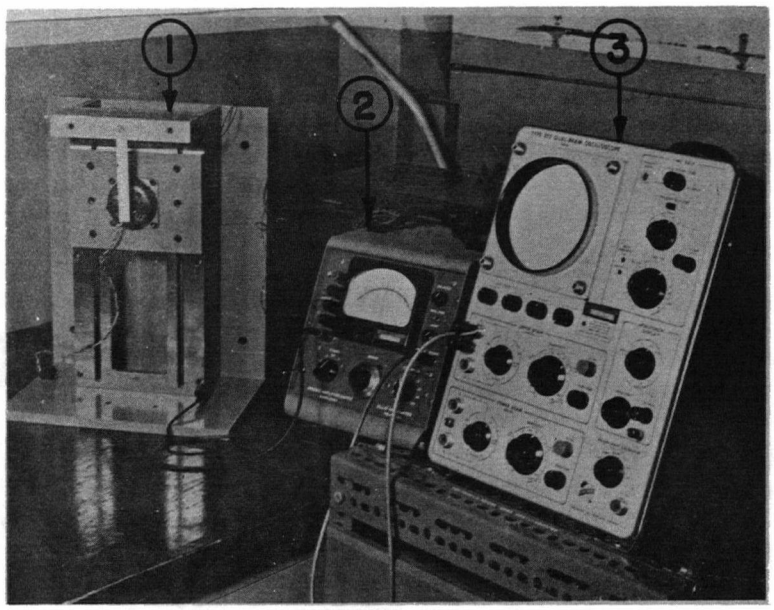

FIGURE 21

CALIBRATION EQUIPMENT

LIST OF COMPONENTS

(1) vibration generator and specimen

(2) BAM

(3) oscilliscope

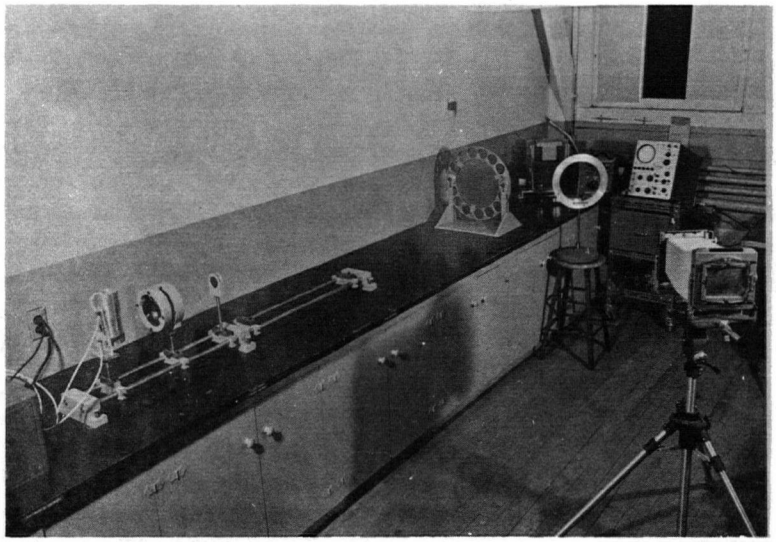

FIGURE 22

SHADOW MOIRÉ ARRANGEMENT

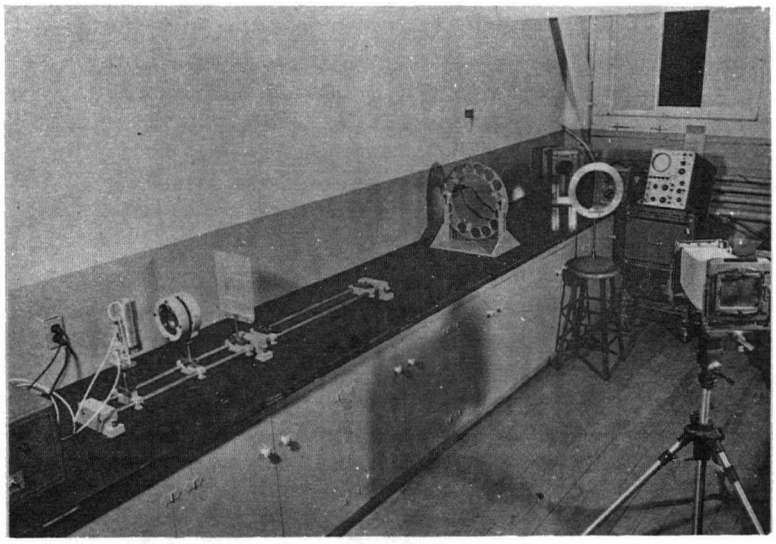

FIGURE 23

SALET-IKEDA ARRANGEMENT

CHAPTER IV

EXPERIMENTAL PROCEUDRE

I. NODE AND DEFLECTION ANALYSIS USING THE SHADOW MOIRÉ METHOD

System Alignment

It has previously been shown in Chapter II that for sharp clear shadows to exist underneath the master grid perfectly parallel light is required. The quality of the moiré patterns therefore is very much dependent upon how accurately the optical system is aligned. In practice, however, perfect alignment is impossible due to the imperfections in the lenses and the inability to obtain a point light source. These stray effects may none the less be minimized. Since the location of the camera, lens L_2 and the grid have no effect on the parallelism of the incident light on the specimen these components will not enter into the following discussion.

The first step in the aligning procedure was to roughly position the geometric centre of all the components along a common axis. This was done quite easily by measuring from a common datum to the centre line of each component. In aligning the light source, condenser and diaphragm the quantity of light passing through the diaphragm into the field lens L_1 was maximized by placing the light source at a distance from the condenser somewhat less than twice the condenser focal length, as shown in Fig. 24. With the light source in place the iris was

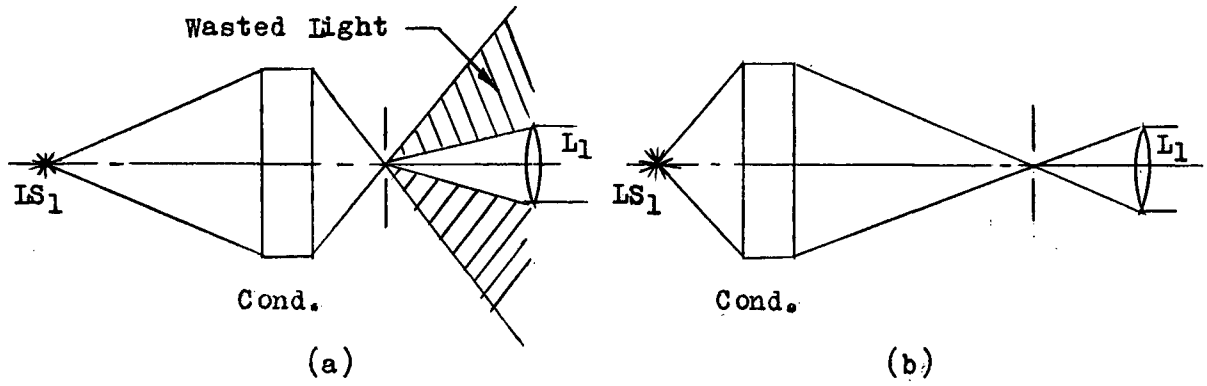

FIGURE 24

ALIGNING THE LIGHT SOURCE

then closed and moved along the optical axis until the image of the light source was seen clearly on the iris. These components were then all locked in place.

With the iris still closed down to its smallest aperature the field lens was relocated such that the focal point of the lens and iris aperature were coincident. A plane mirror was then placed in the collimated light field, downstream of the field lens but facing back toward the light source. Finally, the field lens was adjusted until the reflected image of the light-filled aperature fell directly on the aperature itself. This procedure guaranteed highly collimated light emerging from the field lens.

Positioning the Master Grid

In the previous section it was noted that the quality of the moiré patterns was directly dependent upon the degree of collimation of the incident light. However, before moiré patterns are actually observed, the light must pass through the master grid and thus it can be

seen that the grid may be used as a method of controlling the type of pattern placed on the plate. Consequently the positioning of the grid is of the utmost importance.

In the investigation it was found that the grid could be made to vary three parameters:

(a) contrast

(b) fringe density

(c) fringe orientation with respect to the specimen

Unfortunately, the best of all three of these parameters could not be obtained at the same time. For instance, high fringe density resulted in low contrast and vice versa. The deciding factor in most of the studies was fringe orientation. For the nodal studies it was desirable to cover the plate with an initial field of straight fringes at approximately 45 degrees to the horizontal. This was achieved by first placing the grid such that it was everywhere parallel to the plate; no fringes could be observed. The grid was then tilted slightly with respect to the plate until a desired density of horizontal fringes appeared. By means of the fine adjustment screws the grid was then rotated in the horizontal plane with the result that the fringes rotated. This was continued until the lines were at approximately 45 degrees to the horizontal. The reason for choosing 45 degrees was that it gave a fairly uniform coverage of the plate and nodes were readily detected. For the displacement study using stroboscopy it was not desirable to have the fringes at 45 degrees but rather to have them parallel to one of the

boundaries. This was to aid in interpretation of the fringe patterns. To bring the fringes around parallel to some particular edge it was only necessary to adjust the grid in one plane or the other.

During these adjustments it is assumed that the viewer was either near the focal point of lens L_2 or sufficiently far away from the plate that the light reaching his eye was approximately parallel.

Up to this point nothing has been said regarding the physical orientation of the grid lines, that is, horizontal or vertical. Usually this is determined by the physical layout of the system. If the optical axis of the system is in the horizontal plane the grid lines will be vertical. Such was the case in this study.

Positioning Of The Camera And Lens L_2

Lens L_2 was set at an arbitrary distance from the specimen. The camera lens was located approximately at the focal point of L_2. The exact position was adjusted to: (1) vary fringe density, (2) minimize reflective effects at the plate surface and (3) vary plate image size on the camera screen.

Recording Nodes

Once the initial or static fringe pattern had been established on the plate and the vibration generator adjusted to allow good contact the nodes were ready to be recorded. With the audio generator adjusted

to the desired natural frequency the amplitude was increased until sharp nodes were observed. These were recorded photographically using ASA 400 film at a setting of f/22. Depending on the brightness of the particular pattern being observed the exposure time varied from 5 to 30 seconds.

Recording Displacements

The light source was replaced by the stroboscope as previously described. The strobe was then adjusted to the same frequency as that of the natural frequency of the plate. After ensuring that a suitable initial pattern covered the surface the plate was set into motion. Since the light was flashing at the same frequency as the plate no fringe motion was observed, however, as the frequency of the strobe was varied a beating phenomenon was encountered and the fringes travelled across the plate. The velocity of the fringe movement depended upon the difference between the strobe and vibration frequencies and since both instruments were relatively drift free it could be controlled with ease. To record the displacements at any time the camera was triggered at the desired instant. The film was ASA 3000 Polaroid and the setting f/11. The approximate exposure time was 2 seconds.

Calibration Of The Cantilever Beam

The method of calibrating the cantilever beam has been fully discussed in Chapter II and only the physical details will be dealt with here.

To record the strain in the beam one active and one dummy strain gauge were used. The active gauge was bonded as close as possible to the clamped end on the back of the beam. The dummy was mounted on a piece of plexiglass and attached to the steel base close to the beam. The two gauges acting together formed half of a Wheatstone Bridge circuit, the other half being inside the BAM. The amplified signal from the BAM was recorded on the oscilliscope.

Since it was desired to read dynamic displacements directly off the oscilliscope a known static load was applied to the end of the beam. The resulting signal represented a calculable static displacement anywhere along the length of the beam. By then adjusting the BAM gain and choosing a suitable range on the scope, the scope could be made to read the exact displacement. The scale chosen in this study was .005"/cm. division on the scale. This allowed sufficient latitude in choice of input amplitudes.

Because of the low frequencies involved and also the need to balance the circuitry the oscilliscope was operated in the DC mode. It was found also, that in order to minimize noise amplification the steel base had to be grounded.

Chladni Patterns

To provide experimental proof of the actual existence of nodes Chladni patterns were used. These were formed quite easily by placing

the plates in a horizontal position, exciting them at resonance and then sprinkling them with sand. The sand gravitated toward the nodes and yielded highly definable patterns.

II. ANTINODE ANALYSIS USING THE SALET-IKEDA METHOD

System Alignment

The alignment of the Salet-Ikeda apparatus was a much simpler undertaking than for the shadow moiré, especially since quantitative results were not sought. The light source, with target in place, was set up as shown in Fig. 17. By shifting the ground glass along the optical axis a fairly uniform and intense light field could be made to cover the entire target. Once this had been achieved the components were locked in place. Field lens L_1 was then moved to a position at which its focal point coincided with the centre of the target. This completed alignment of the incident light.

In order to align the remainder of the system one of the plate specimens had to be placed at some convenient position along the optical axis of the incident light. By then rotating the plate through some suitable angle the reflected light could be directed into lens L_2. The camera then, with its diaphragm closed right down, was placed at the focal point of lens L_2. After slight vertical and horizontal adjustment a clear image of the target could be observed. The system was then ready to record antinodes.

Choice of Target

Throughout the tests only straight line targets were used. There was, however, no particular reason for this other than to aid in interpretation. Because of the nature of the technique quite arbitrary patterns of lines could be made to yield equally good results. The density of the target lines, however, was most important and it was found that a target of 20 lpi or more could not be used since poor contrast resulted. Therefore all the tests were run with either one of the two remaining targets. The method adopted was to set up the plate with one particular target and then check the image of the target on the ground glass of the camera for contrast and density. If the pattern wasn't satisfactory the other grid was substituted. It was found that a reasonable pattern could always be achieved with one grid or the other.

Recording Antinodes

It has previously been shown that the antinode lies at the intersection of any two partial antinodes and therefore, for any one natural frequency being investigated photographs must be taken with the target lines in two different directions. In this study it was found that placing the target vertically for one photograph and horizontally for the other was the easiest to perform. In the case of the beam only one dimensional wave motion existed and hence it was only necessary to use one grid. This was placed horizontally so as to be able to record slopes taken in a direction along the beam.

When the plate was excited at resonance and the antinodes were being studied it was noticed that quite often the partial antinodes occurred at a point or line at which the pattern was rather poor. In fact, it occasionally happened that a partial antinode fell across a point at which there was no pattern at all, in which case the partial antinode went undetected. To remedy this situation it was necessary to "scan" the plate by making minute horizontal or vertical adjustments in the position of the pinhole. This was done quite easily by using the vernier adjustments on the camera tripod. In this manner a suitable pattern could be found that would locate all the partial antinodes.

Another problem encountered in studying the patterns was the appearance of wide bands of yellow and blue light between the dark fringes. This tended to grey the negatives and hence give poor pictures. The situation was greatly improved by using a Kodak #58 (B) filter.

CHAPTER V

EXPERIMENTAL RESULTS

I. NATURAL FREQUENCIES

The calculated and observed natural frequencies of the beam and plates are given in Table 1. In determining these frequencies three material properties E, ν and ρ were required. These were found experimentally, E and ν by simple tensions tests and ρ by weighing a known volume. The values were:

$$E = 560{,}000 \text{ psi}$$

$$\nu = 0.39$$

$$\rho = 1.01 \times 10^{-4} \frac{\text{lb sec}^2}{\text{in}^4}$$

MODE	CANTILEVER BEAM		SQUARE PLATE		CIRCULAR PLATE	
	CALCULATED	OBSERVED	CALCULATED	OBSERVED	CALCULATED	OBSERVED
1	44 Hz	48 Hz	46 Hz	43 Hz	147 Hz	143 Hz
2	281 "	310 "	113 "	108 "		
3	780 "	850 "	283 "	270 "		
4	1530 "	-	363 "	346 "	576 "	620 "
5	2520 "	-	413 "	394 "		
8					1680 "	1650 "

TABLE 1

NATURAL FREQUENCIES

II. TABLE OF PHOTOGRAPHIC RESULTS

The following pages include all the pictures that were taken of the beam and two plate specimens. For the purpose of comparison a theoretical solution or sand pattern is given directly opposite each photograph of the nodal patterns. For the antinodes, however, a theoretical solution is given only for the beam. At the end of the results an arbitrary shape is investigated to locate its nodes and antinodes for particular natural frequencies. The photographs are listed as follows:

NODES

SPECIMEN	MODE	FREQ.	FIGURE
CANTILEVER BEAM	Static	-	25 (a)
	1	48 Hz	25 (b)
	2	310 "	25 (c)
	3	850 "	25 (d)
SQUARE PLATE	Static	-	27 (a)
	1	43 Hz	27 (b)
	2	108 "	27 (c & d)
	3	270 "	27 (e & f)
	4	346 "	27 (g & h)
CIRCULAR PLATE	Static	-	30 (a)
	1	143 Hz	30 (b & c)
	4	620 "	30 (d & e)
ARBITRARY SHAPE		420 "	35 (a)

ANTINODES

SPECIMEN	MODE	FREQ.	FIGURE
CANTILEVER BEAM	Static	-	26 (a)
	1	48 Hz	26 (b)
	2	310 "	26 (c)
	3	850 "	26 (d)
SQUARE PLATE (grid in x direction)	Static	-	28 (a)
	1	43 Hz	28 (c)
	2	108 "	28 (e)
	3	270 "	28 (g)
	4	346 "	28 (i)
	5	394 "	28 (k)
SQUARE PLATE (grid in y direction)	Static	-	28 (b)
	1	43 Hz	28 (d)
	2	108 "	28 (f)
	3	270 "	28 (h)
	4	346 "	28 (j)
	5	394 "	28 (m)
CIRCULAR PLATE	Static	-	31 (a)
	4	620 Hz	31 (b)
	8	1650 "	31 (c)
ARBITRARY SHAPE (grid in n direction)		600 "	35 (b)
ARBITRARY SHAPE (grid in x direction)		600 "	35 (c)
Superposition of partial antinodes (square plate)			29

DISPLACEMENTS

SPECIMEN	MODE	FREQ.	FIGURE
CANTILEVER BEAM			
Positive Displacement	1	48 Hz	32 (a)
Static			32 (b)
Negative Displacement	"	"	32 (c)
Actual Arrangement			32 (d)
Dynamic Displacement Curve			32 (e)
SQUARE PLATE			
Static			33 (a)
Positive Displacement	4	346 Hz	33 (b)
Negative Displacement	"	"	33 (c)
CIRCULAR PLATE			
Static			34 (a)
Positive Displacement	1	143 Hz	34 (b)
Negative Displacement	"	"	34 (c)

(a) STATIC PATTERN

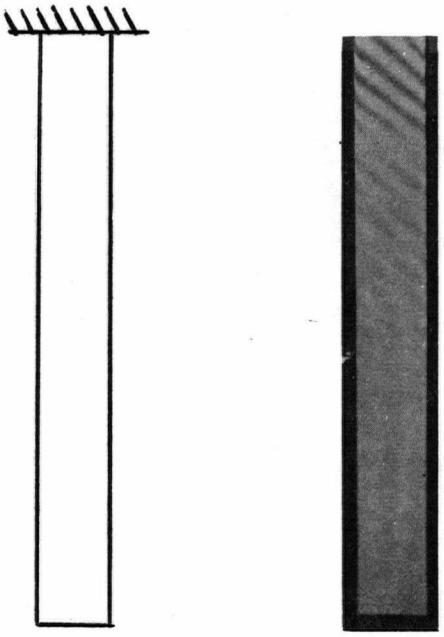

(b) 1st MODE

(48 Hz)

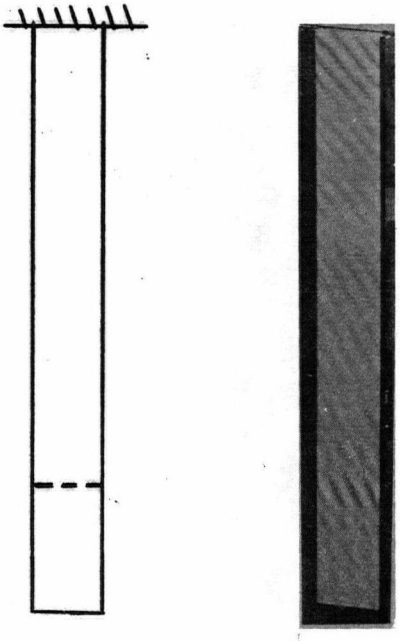

(c) 2nd MODE

(310 Hz)

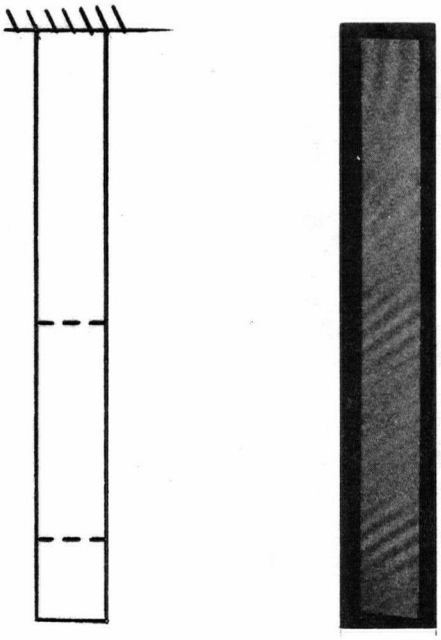

(d) 3rd MODE

(850 Hz)

FIGURE 25

NODES IN A CANTILEVER BEAM

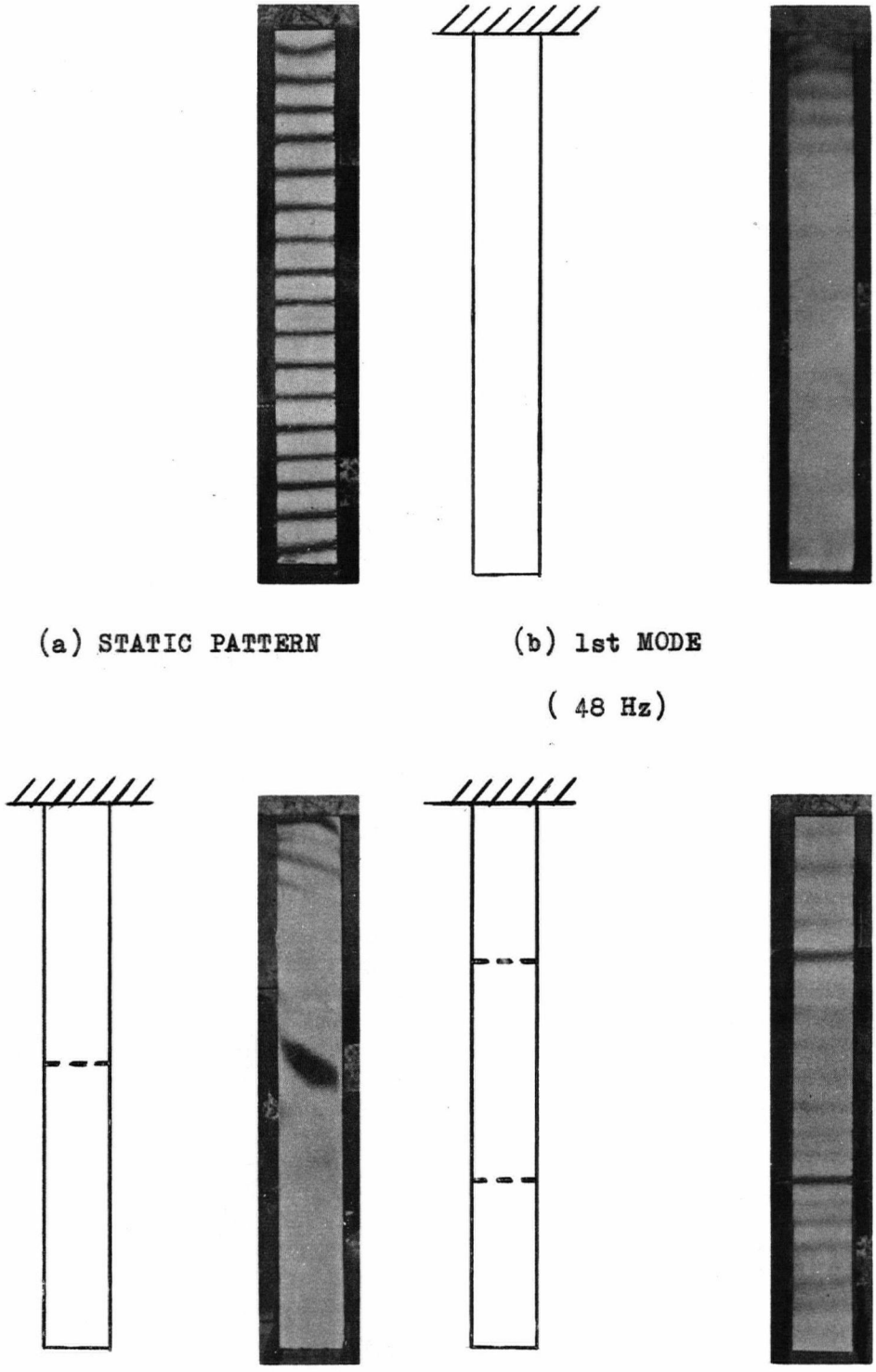

(a) STATIC PATTERN

(b) 1st MODE

(48 Hz)

(c) 2nd MODE

(310 Hz)

(d) 3rd MODE

(850 Hz)

FIGURE 26

ANTINODES IN A CANTILEVER BEAM

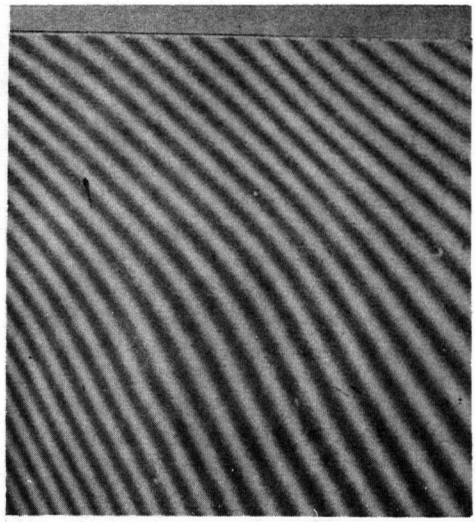

(a)

STATIC PATTERN

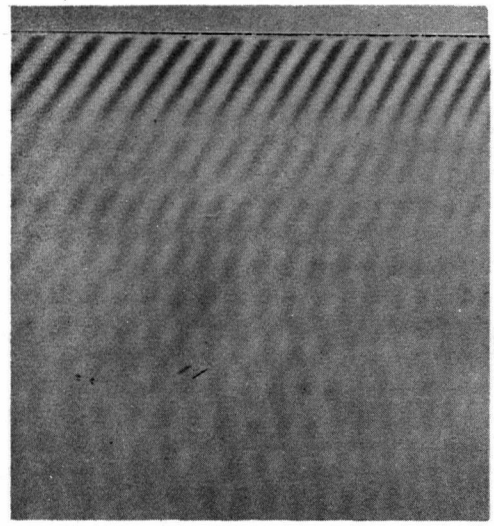

(b)

1st MODE

(43 Hz)

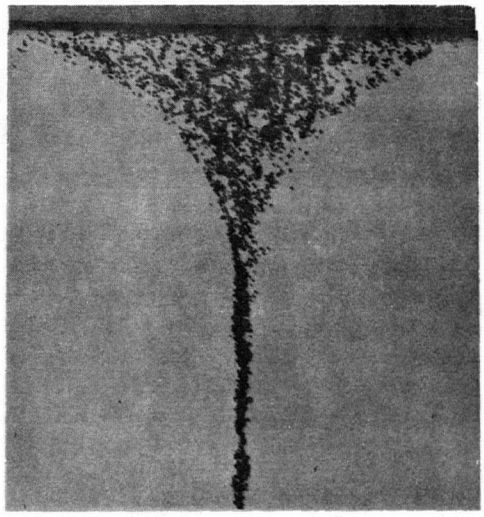

(c)

2nd MODE - SAND

(108 Hz)

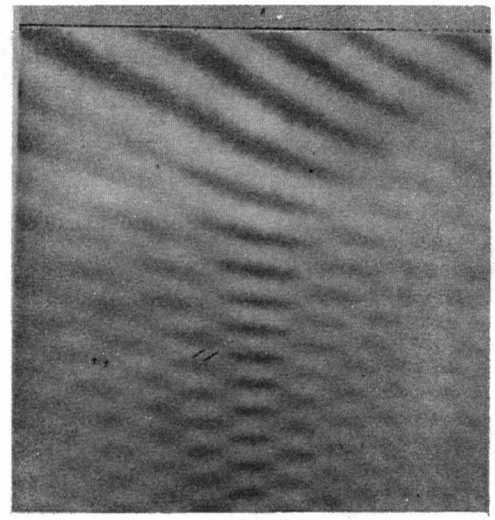

(d)

2nd MODE

(108 Hz)

FIGURE 27

NODES IN A SQUARE PLATE

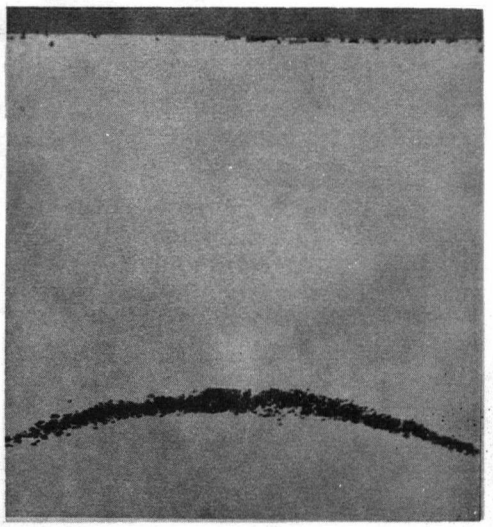

(e)

3rd MODE - SAND

(270 Hz)

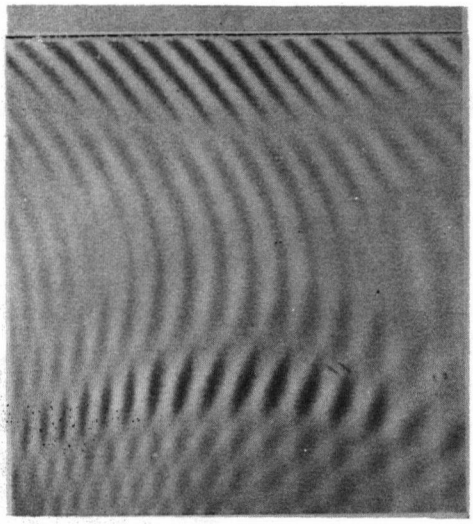

(f)

3rd MODE

(270 Hz)

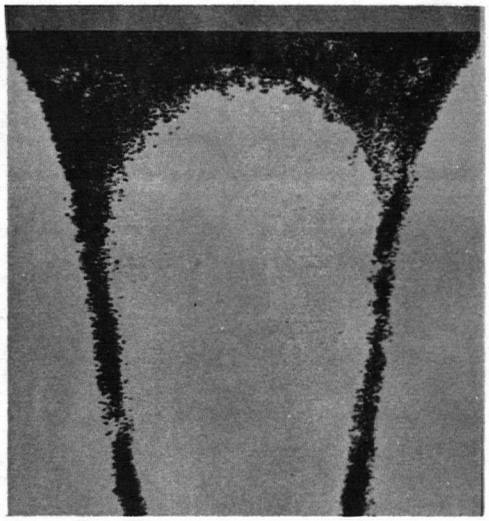

(g)

4th MODE - SAND

(346 Hz)

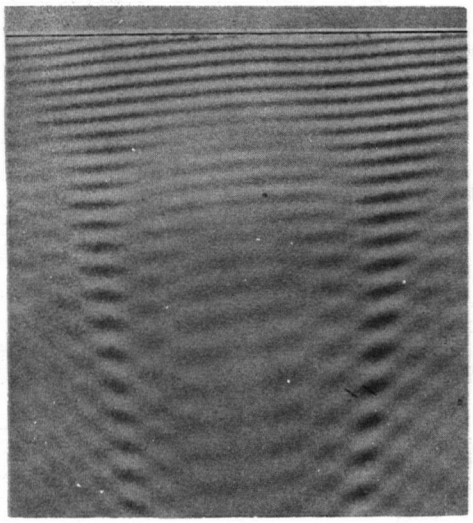

(h)

4th MODE

(346 Hz)

FIGURE 27

NODES IN A SQUARE PLATE

TARGET DIRECTION 

TARGET DIRECTION 

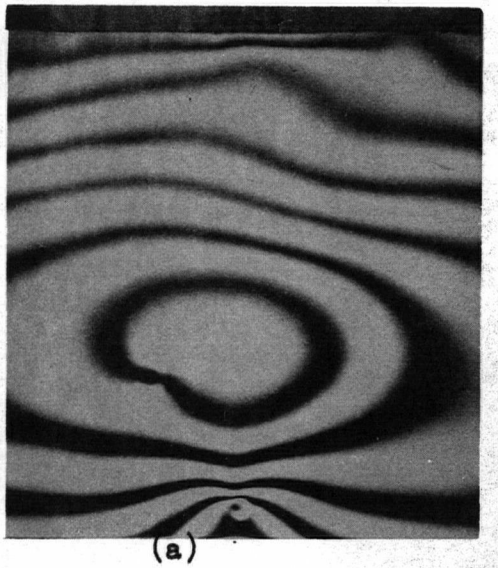

(a)

STATIC PATTERN

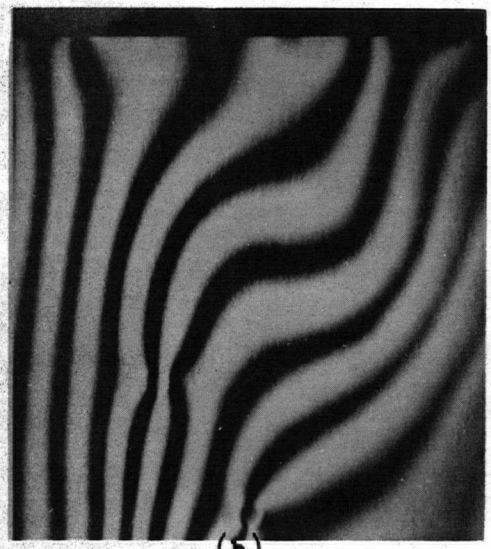

(b)

STATIC PATTERN

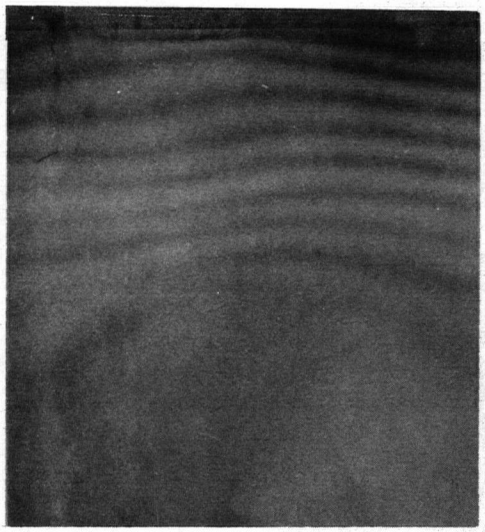

(c)

1st MODE

(43 Hz)

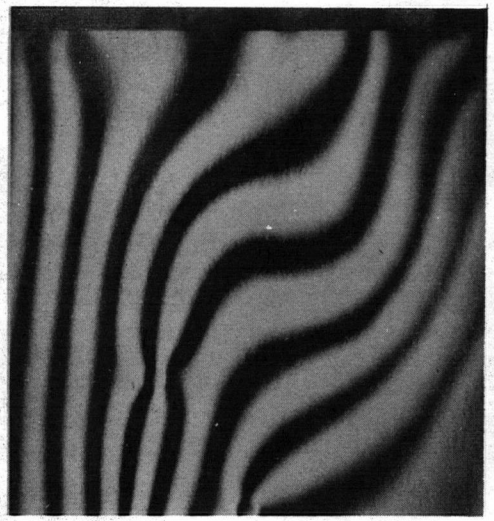

(d)

1st MODE

(43 Hz)

FIGURE 28

PARTIAL ANTINODES IN A SQUARE PLATE

TARGET DIRECTION 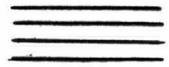

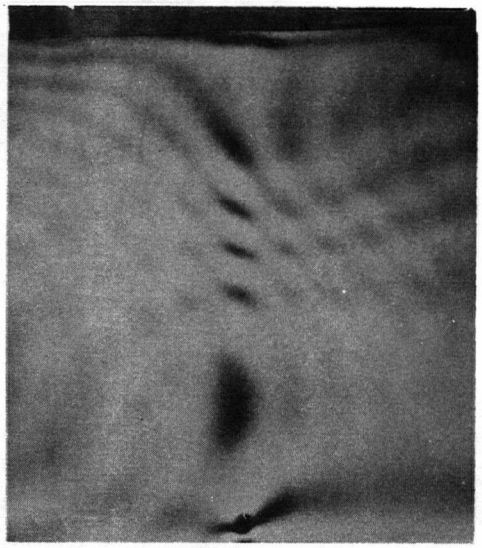

(e)

2nd MODE

(108 Hz)

TARGET DIRECTION 

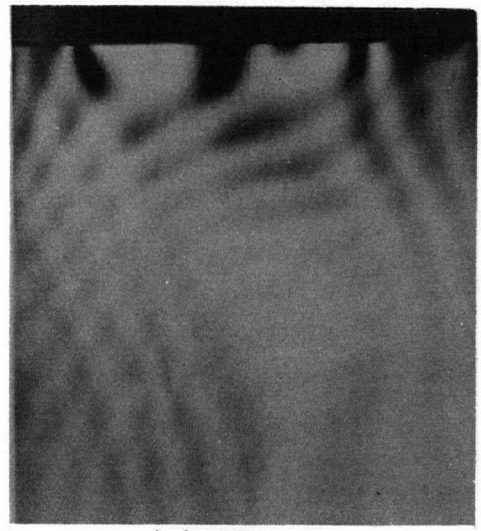

(f)

2nd MODE

(108 Hz)

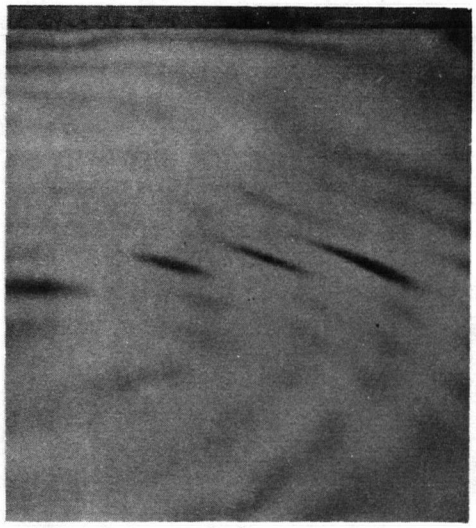

(g)

3rd MODE

(270 Hz)

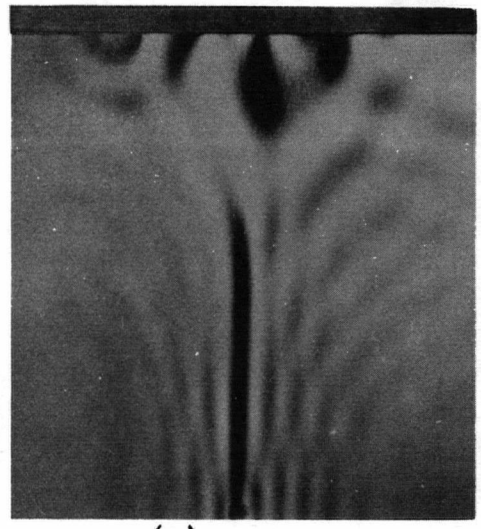

(h)

3rd MODE

(270 Hz)

FIGURE 28

PARTIAL ANTINODES IN A SQUARE PLATE

TARGET DIRECTION 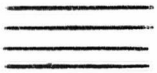

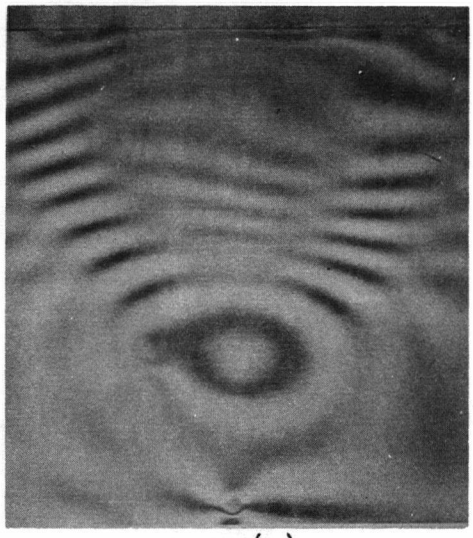

(i)

4th MODE

(346 Hz)

TARGET DIRECTION 

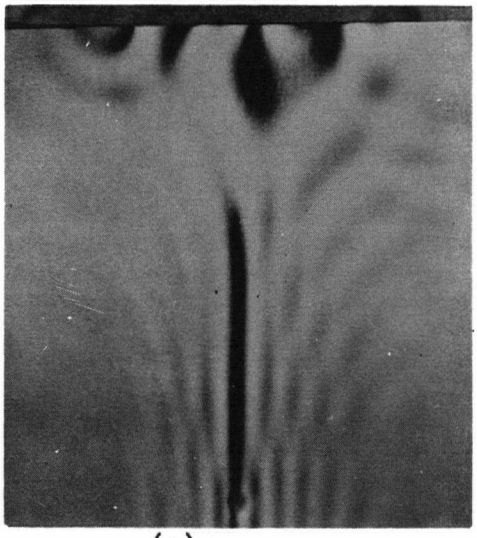

(j)

4th MODE

(346 Hz)

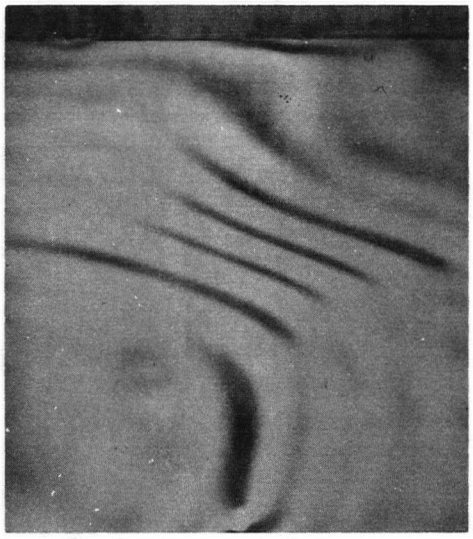

(k)

5th MODE

(394 Hz)

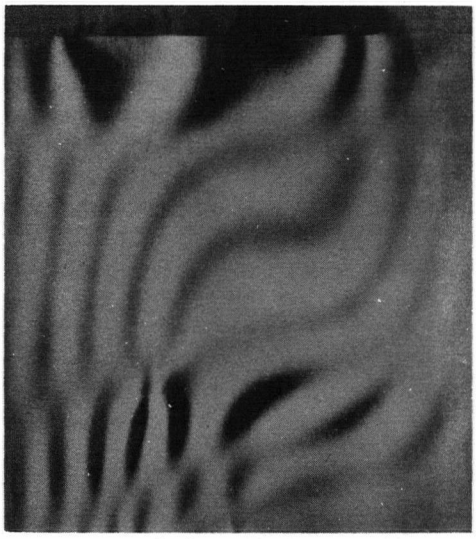

(m)

5th MODE

(394 Hz)

FIGURE 28

PARTIAL ANTINODES IN A SQUARE PLATE

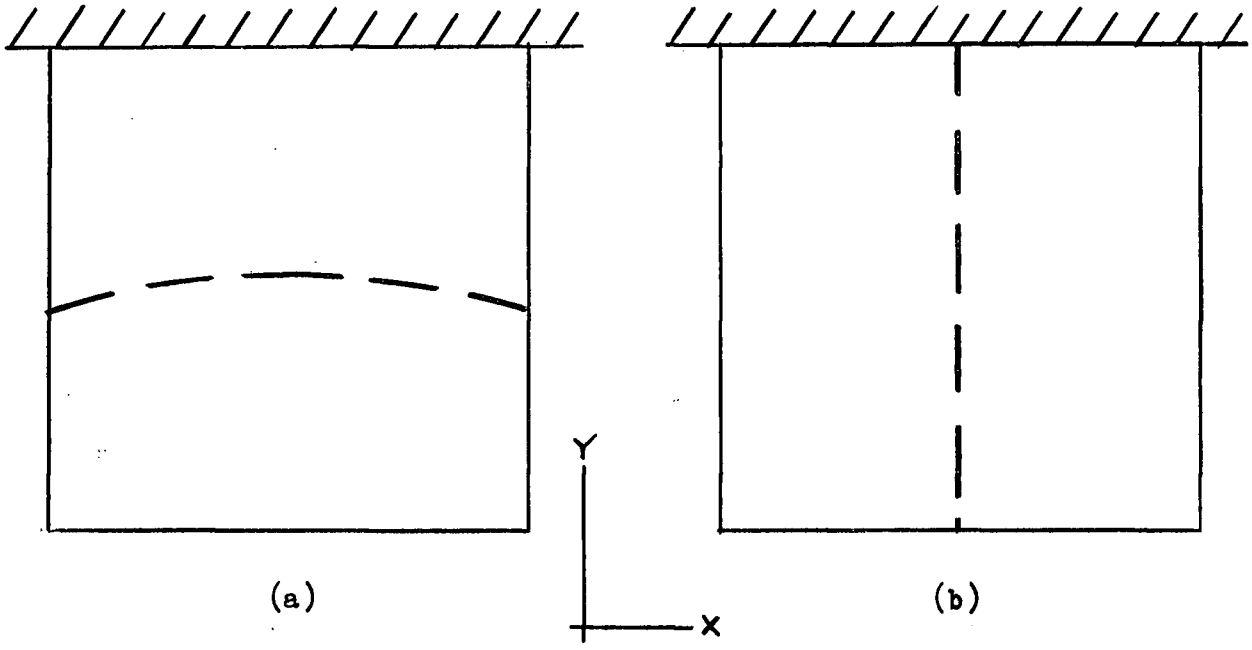

(a)

3rd MODE, PARTIAL ANTINODE

IN Y DIRECTION

(b)

3rd MODE, PARTIAL ANTINODE

IN X DIRECTION

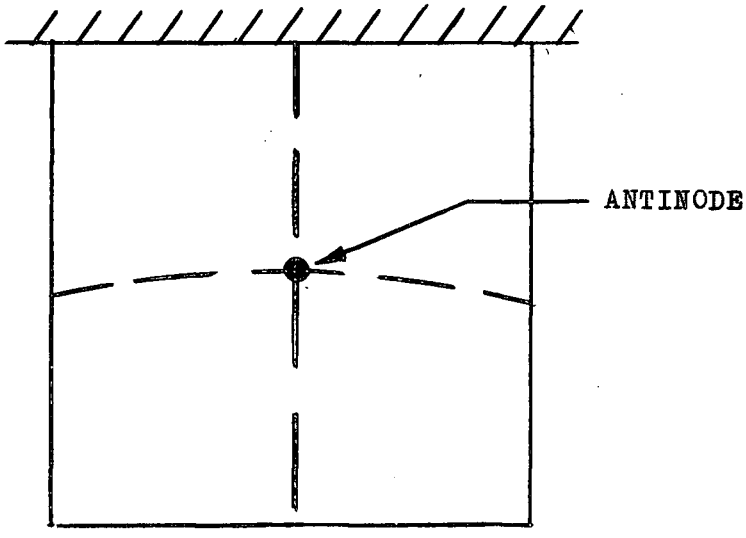

(c)

SUPERPOSITION OF PARTIAL ANTINODES

FIGURE 29

SUPERPOSITION OF TWO PARTIAL ANTINODES

TO LOCATE THE TRUE ANTINODE

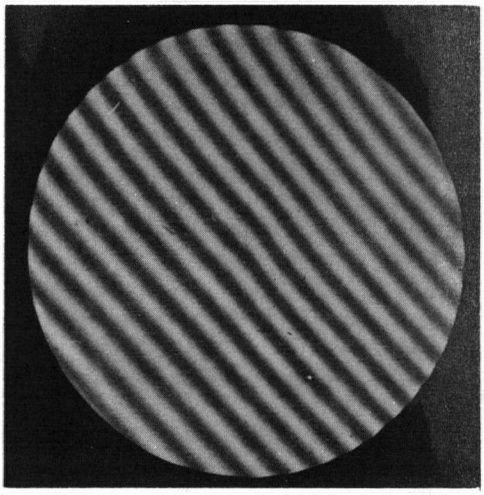

(a)

STATIC PATTERN

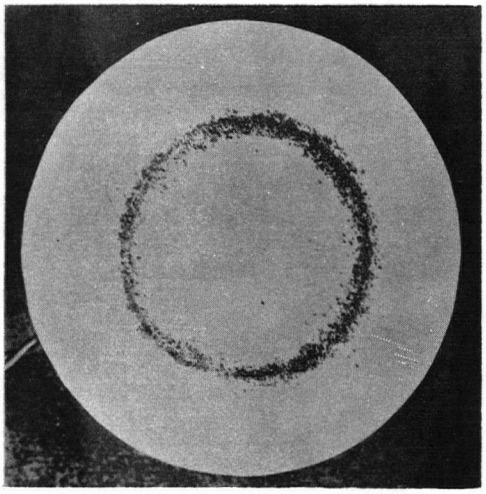

(b)

1st MODE - SAND

(143 Hz)

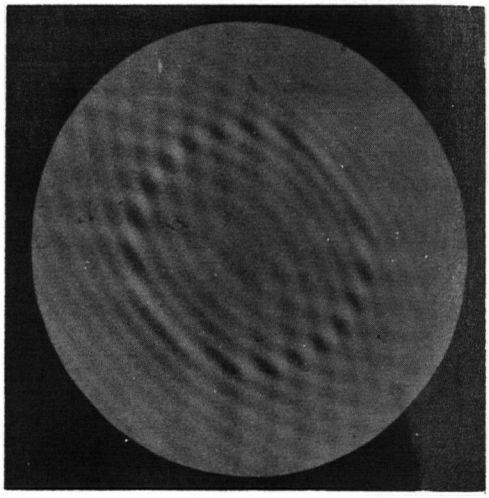

(c)

1st MODE

(143 Hz)

FIGURE 30

NODES IN A CIRCULAR PLATE

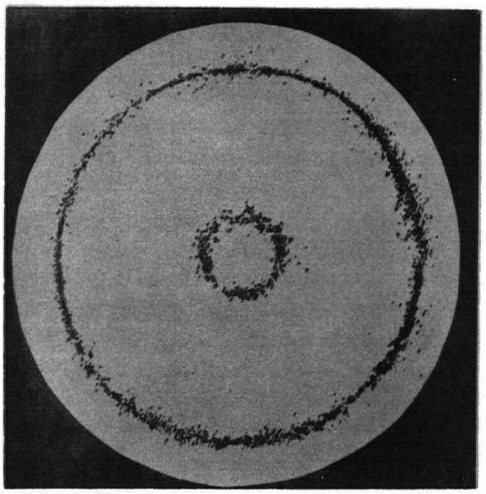

(d)

4th MODE - SAND

(620 Hz)

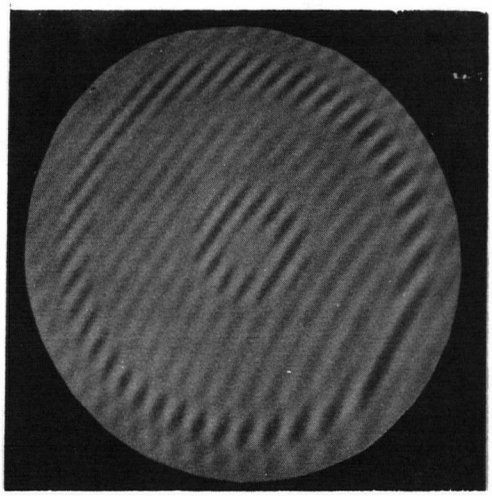

(e)

4th MODE

(620 Hz)

FIGURE 30

NODES IN A CIRCULAR PLATE

TARGET DIRECTION

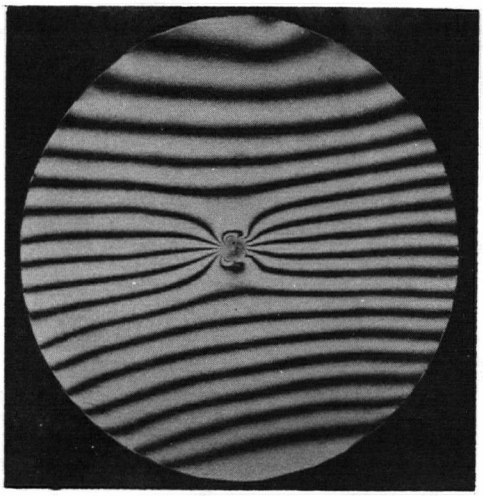

(a)

STATIC PATTERN

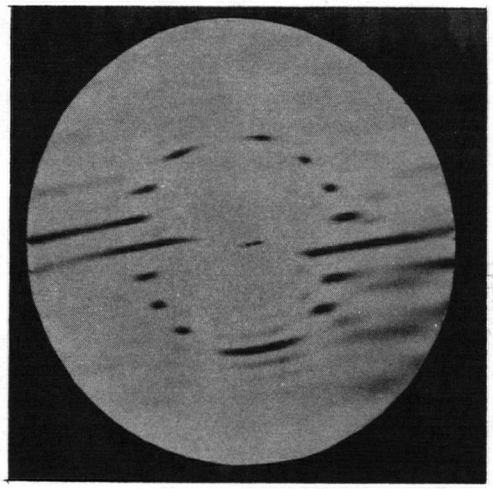

(b)

4th MODE

(620 Hz)

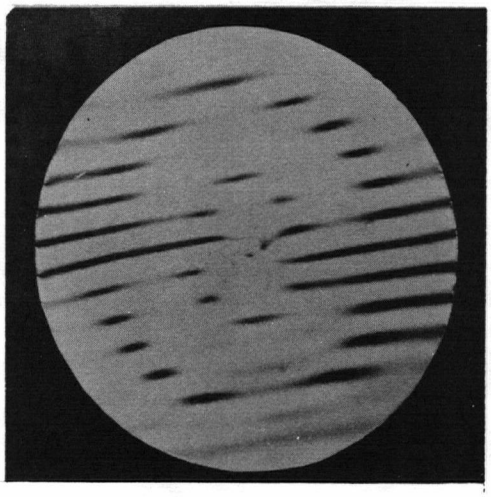

(c)

8th MODE

(1620 Hz)

FIGURE 31

ANTINODES IN A CIRCULAR PLATE

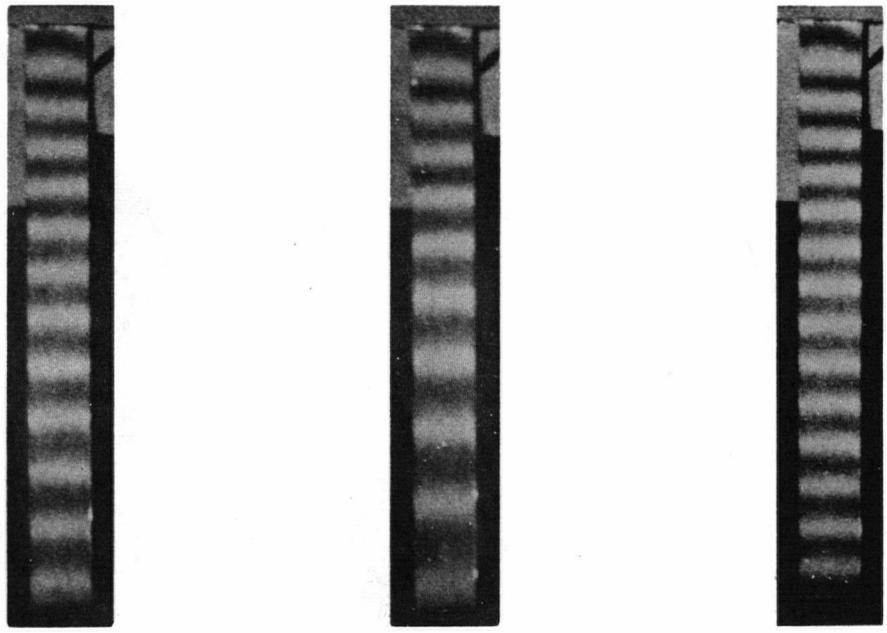

(a) POSITIVE DISPLACEMENT

(b) STATIC PATTERN

(c) NEGATIVE DISPLACEMENT

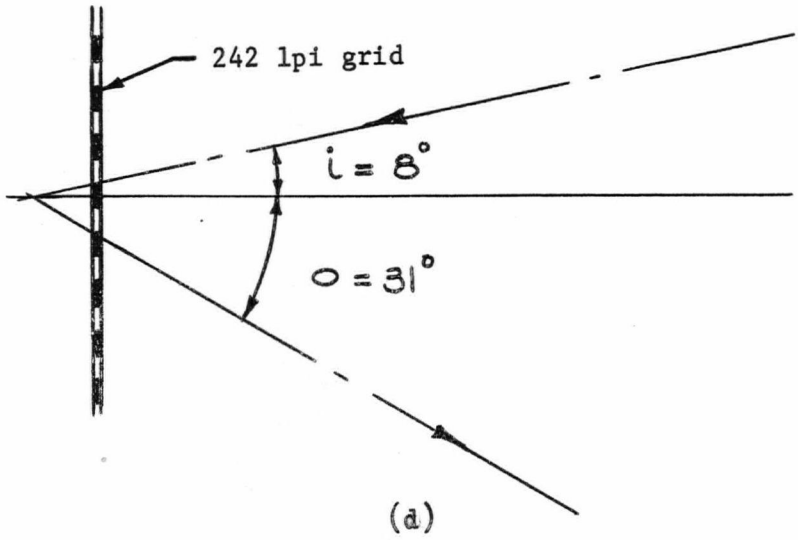

(d)

ACTUAL ARRANGEMENT

FIGURE 32

DISPLACEMENTS IN A CANTILEVER BEAM

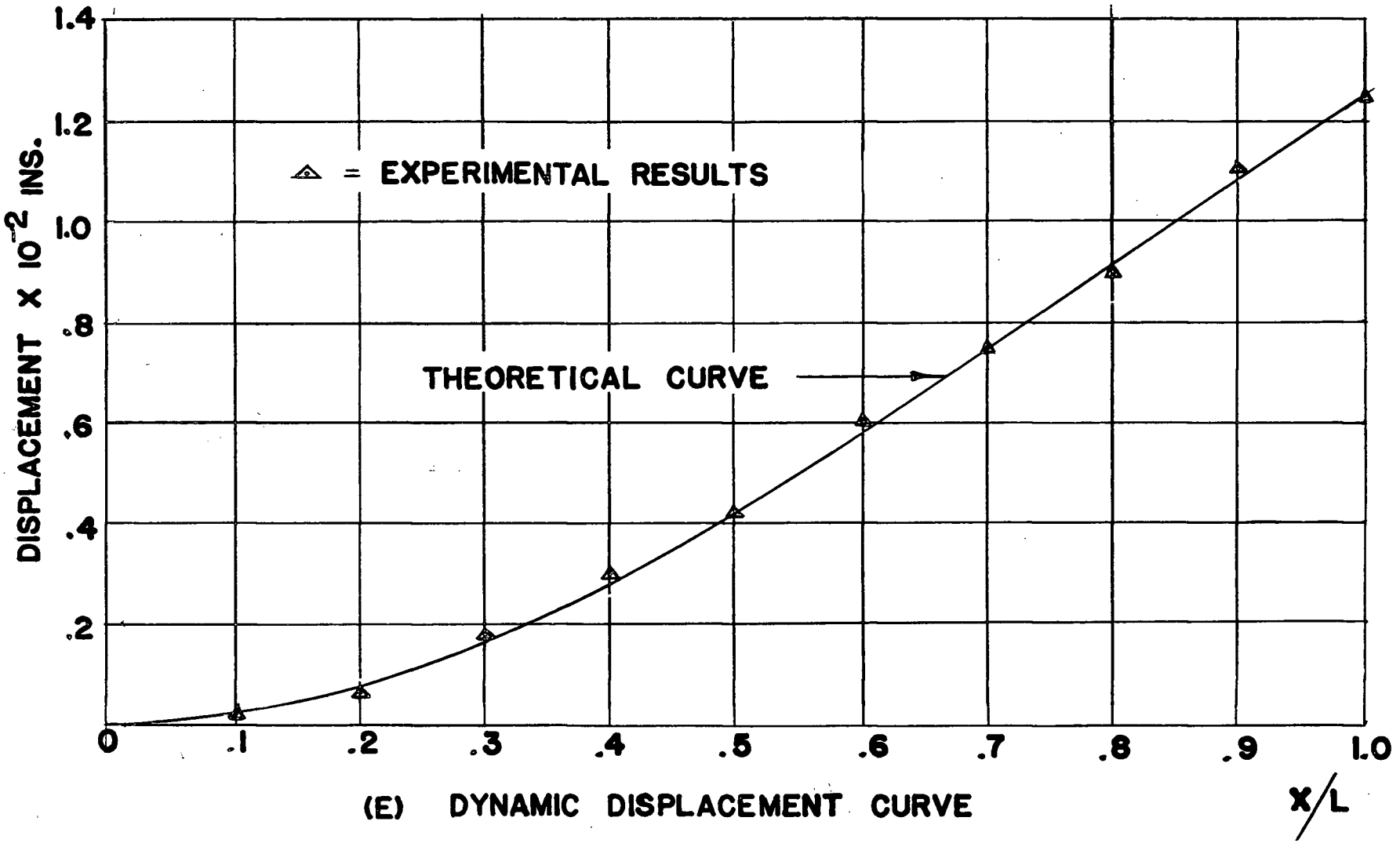

(E) DYNAMIC DISPLACEMENT CURVE

FIGURE 32

DISPLACEMENTS IN A CANTILEVER BEAM

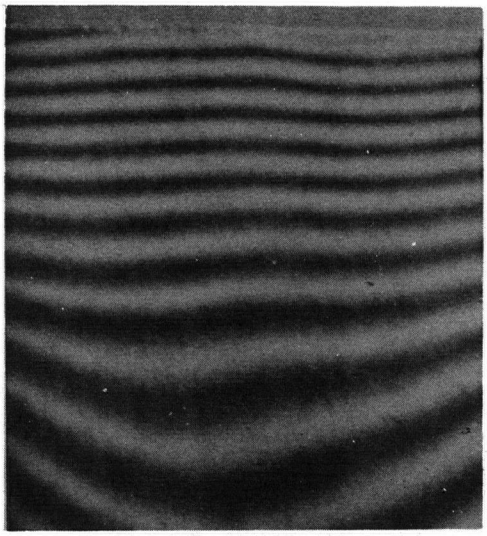

(a)

STATIC PATTERN

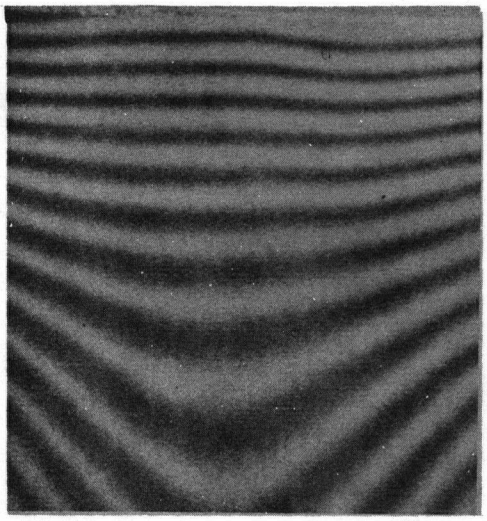

(b)

POSITIVE DISPLACEMENT, 4th MODE

(346 Hz)

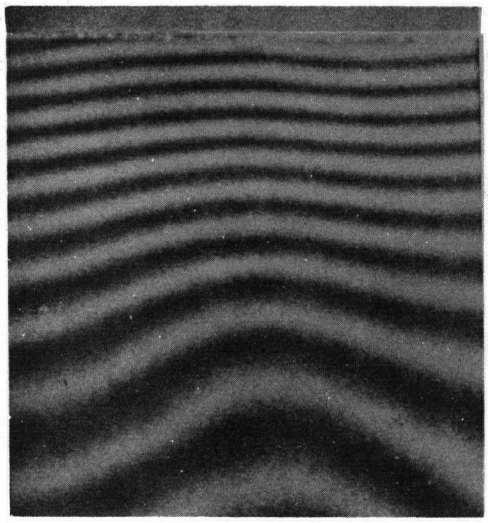

(c)

NEGATIVE DISPLACEMENT, 4th MODE

(346 Hz)

FIGURE 33

DISPLACEMENTS IN A SQUARE PLATE

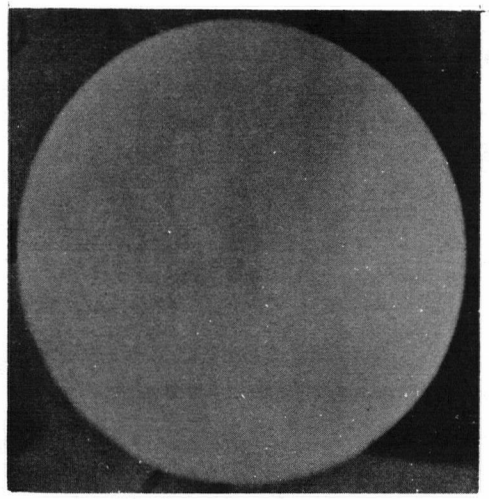

(a)

STATIC PATTERN

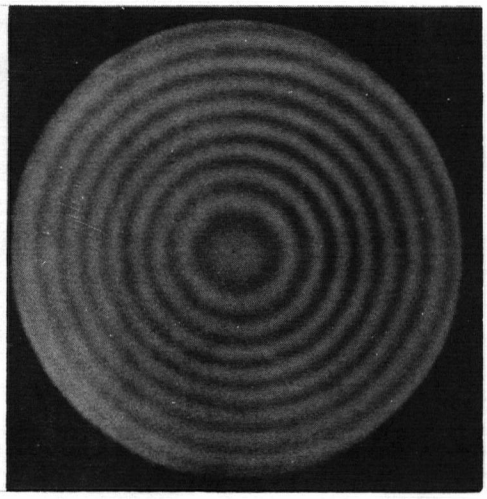

(b)

POSITIVE DISPLACEMENT, 1st MODE

(143 Hz)

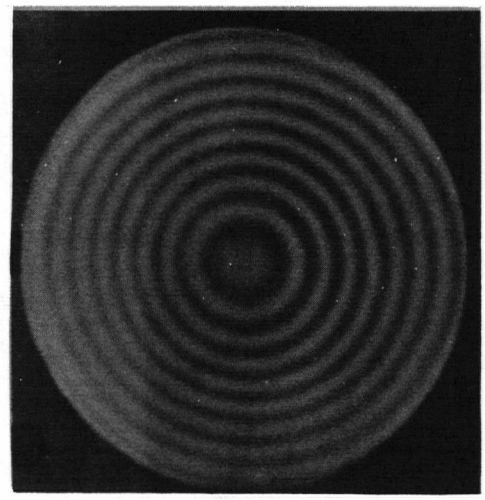

(c)

NEGATIVE DISPLACEMENT, 1st MODE

(143 Hz)

FIGURE 34

DISPLACEMENTS IN A CIRCULAR PLATE

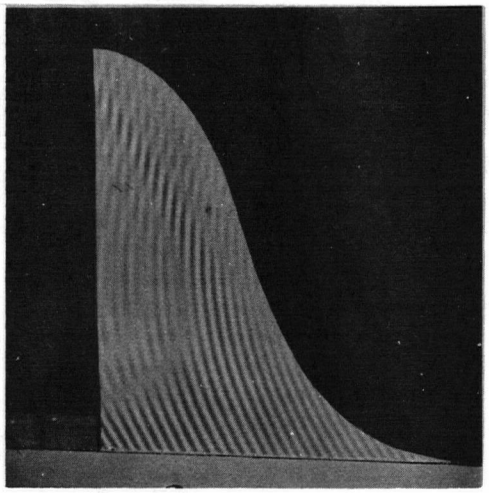

(a)

TYPICAL NODAL PATTERN

(420 Hz)

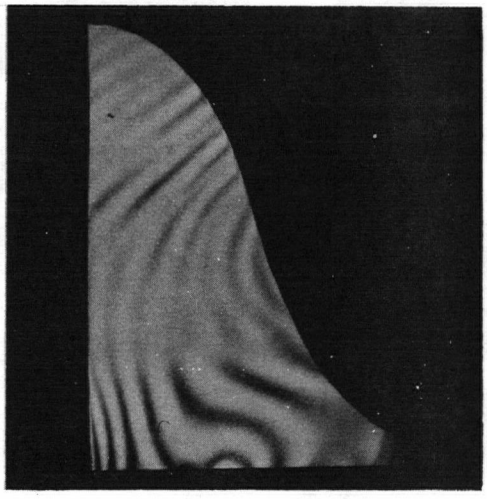

(b)

PARTIAL ANTINODE, TARGET

(600 Hz)

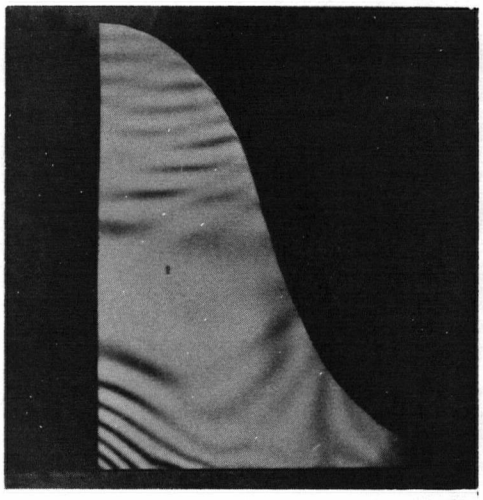

(c)

PARTIAL ANTINODE, TARGET

(600 Hz)

FIGURE 35

NODES AND ANTINODES IN A PLATE OF ARBITRARY SHAPE

CHAPTER VI

DISCUSSION OF RESULTS

I. NODES

Comparison of the sand pattern or theoretical solutions with the moiré patterns obtained in the experiments clearly show that the technique does, in fact, definitely locate the nodal positions. The patterns are clear and distinct and in spite of the vague cross hatch that covers most of the specimens there is no doubt as to which lines actually trace out the nodes. Their distinctness, however, was found to be very dependent upon the density and orientation of the grid and it was thus desirable to apply a rough figure of merit to the system. A good indication was shown to be given by the empirical relation:

$$\frac{w_a}{p} = k \qquad (6.1)$$

For sharp clear nodes a value of k=50 was found to be applicable while a value k=100 yielded visible but rather inferior patterns. For instance if a 200 lpi grid was used and sharp patterns were sought the grid could be placed no further than 1/4" from the plate. From eqn. 6.1 it is seen that if large amplitudes are to be studied and yet maintain good fringe quality it is necessary to employ a much coarser grid. Thus there is no upper limit placed on the technique other than the physical limitations on the size of the apparatus components. This, of course, is subject to the upper bound mentioned in Chapter II in which contrast between the node and remaining washed out pattern becomes important.

The minimum deflection that could be detected with a 500 lpi grid, angles of roughly i=10 degrees and o=20 degrees was from eqn. 2.1;

$$h = \frac{.002}{\tan 10 + \tan 20}$$

$$h = .004''/\text{fringe}$$

and from eqn. 2.8,

$$w_{min} = \frac{h}{4}$$

$$= .001''$$

Thus the technique can detect nodes for any plate having an amplitude of vibration greater than .001". Diffraction effects begin to become significant when grids of smaller pitch are used.

It was shown in the last chapter that if the initial pattern on the plate is oriented at 45 degrees to the horizontal good plate coverage results. However, in many of the photographs the pattern is not at 45 degrees but rather at some other angle. In fact, in some cases it is either completely horizontal or vertical. In these cases it was found that even though a 45 degree pattern yielded a good nodal pattern it could be greatly improved upon by rotating the grid.

As in all techniques involving the use of fringes there arises the problem of determining the exact centre of the fringe lines. In this case, however, not one fringe but rather a band of a family of fringes is involved and therefore methods of fringe sharpening such as the one given by Post (27) cannot be applied here. Since the width of the node

line is amplitude dependent, usually sufficiently good results were obtained by increasing the amplitude to a point just before contrast disappeared. However, when sufficient amplitude could not be imparted to the beam as in Fig. 25 (d) the patterns required considerable interpretation.

II. ANTINODES

The antinodes determined in the case of the cantilever beam compare favourably with theory and it is assumed that the plates do likewise. If in the case of the square plate the nodal patterns are superimposed on top of the antinode patterns they are seen to fill in the gaps as would be expected. For the circular plates this may only be done for the 4th mode.

The initial patterns on the plates are not necessarily an indication of the initial curvatures since the camera was often not placed exactly at the focal point of lens L_2. None the less certain surface discontinuities do show up. For instance, both the circular and square plates show a small circular pattern on the surface. This was due to shrinkage brought about by cementing generator attachments to the back surfaces of the plates.

The method shown for determining the true antinode by superposition of the two partial antinodes as in Fig. 29 works very well but the question arises, why could the negatives not be super-

imposed to achieve the same result photographically? Unfortunately this was not thought of until after all the photographs had been taken. Since many of these were taken from different camera positions they could not be superimposed. This, however, is considered to be the most ideal method for visualizing antinodes and is suggested to anyone performing the study in the future. Another question also arises, if one partial antinode is determined with the target lines in one direction and another partial antinode with the target lines in some other direction why could not both sets of lines be superimposed on the target and in such a manner record both partial antinodes simultaneously? This was attempted but was found to be subject to definite physical limitations in viewing the pattern. This arose from the fact that the curvatures of the two waves at the antinode were not necessarily the same and hence pattern washout occurred at a much lower amplitude in one direction than it did in the other. This had the following effect: at amplitude 1, a partial antinode in say the y direction appeared, the x pattern remaining unaffected. At amplitude 2, which was greater than amplitude 1, the x pattern washed out and produced a partial antinode in the x direction. However, amplitude 2 was so large that the partial antinode in the y direction had been reduced to such a thin line that it was no longer visible. Thus in most cases only one partial antinode was visible at a time. This problem did not, of course, occur if the curvatures at the antinode were the same.

The limits on the technique are very similar to those dis-

cussed for the shadow moiré. The upper limit is difficult to determine since it is a matter of contrast between the partial antinode and the washed out pattern. The lower limit, however, may be determined from eqn. 2.7. As in the case of the nodes the necessary condition for washout is that the fringe shift be greater than 1/2 a fringe width or in other words the minimum slope change is:

$$\vartheta_{min} = \frac{\vartheta}{4}$$

$$= \frac{1}{8} \tan^{-1} \frac{r}{F_1}$$

Taking typical values as r=.1", F_1=60" it can be seen that ϑ_{min} = .0002 rads. This then becomes the lower limit on the technique using the above apparatus.

III. DISPLACEMENT

The displacements in the cantilever beam are given in Fig. 32 (a) - (c) along with measured angles of the system in Fig. 32 (d). The peak to peak input displacement at the free end of the beam in this particular case was .025" as read off the oscilliscope. By counting fringes to the nearest 1/4 fringe it is seen that the static pattern has 13 fringes, the positive deflection pattern 10 3/4 fringes and the negative deflection pattern 15 1/4 fringes. This represents a peak to peak fringe change of 4 1/2 fringes and the total displacement is thus given by:

$$w = 4.5\ h$$

$$= 4.5 \frac{\frac{1}{242}}{\tan 8^\circ + \tan 31^\circ}$$

$$= .0252''$$

This value is exceptionally close to the input amplitude and serves to demonstrate the validity of the technique as a dynamic displacement measuring technique. The fact that they are so close is partly coincidental because of the various errors in both the measuring and calibration methods. The major errors are as follows:

Error in reading angles	$1/2^{\circ}$ in 40°	1.2%
Error in reading fringes	1/4 in 13	2.4%
Error in calibration	.001" in .025"	4.0%
Total error		7.6%

The experimental displacements in the square and circular plates have not been evaluated but are included for completeness. In the circular plate no initial pattern is placed on the surface so that displacements may be evaluated directly without the need of subtracting the initial pattern.

IV. SECOND ORDER EFFECTS

In both the nodal and antinodal patterns if can be seen that a secondary background fringe pattern of low intensity appears on most plates. Since the response of a generic point in the plate is harmonic, i.e. $x = A \sin \omega t$

and,

$$\frac{dx}{dt} = A\omega \cos \omega t$$

it can be seen that as ωt approaches $\pi/2$ the velocity of the plate ap-

proaches zero. Since the fringe velocity is directly related to the plate velocity it is observed that it must likewise apprach zero. Hence a motionless fringe condition, i.e. fringe "dwell", results at both amplitude peaks. Although this condition is momentary it is sufficient to leave a faint impression on the eye or camera and thus the secondary pattern on the plate is the superposition of the two maximum amplitude fringe patterns on the plate. In some instances the secondary fringe patterns are of high enough density to actually produce a secondary moiré pattern, or a "moiré of a moiré". This can be clearly seen in Fig. 27 (h) in which concentric horseshoe shaped patterns are enclosed by the primary nodal pattern.

V. GENERAL OBSERVATIONS

One point which generally plagued the study throughout its entirety was the method of introducing vibration into the plates. This difficulty arose from the fact that, because of stiffening effects, no physical attachment could be provided between the plate and generator spindle. This meant that to excite the plate it was necessary to place the generator spindle in close contact with the plate surface. Two major problems occurred because of this: (1) if a large amplitude was introduced the spindle would tend to "buzz" on the plate and introduce second order harmonics which washed out the entire pattern; (2) if the plate was driven at a nodal point it was impossible to excite that particular mode. The first of these problems was eliminated by keeping

the amplitude low enough so that buzzing did not occur. This presented a limitation on the technique because in many cases, for instance Fig. 25 (d), the amplitude could not be increased sufficiently to yield sharp definable nodes. The second problem was overcome by shifting the spindle to different points on the plate and thus ensuring that it was not being driven at a node.

For the circular plate a different situation arose. Since the spindle was physically attached to the plate no buzzing resulted and the plate could be driven to any desired amplitude. However, because it was being driven at the centre no modes containing radial nodes could be excited.

CHAPTER VII

SUMMARY AND CONCLUSIONS

I. SUMMARY

It was the intention of this investigation to extend the use of optical techniques to the study of vibrating plates subject to relatively large displacements. Three vibrational characteristics were sought: (1) the location of the nodes; (2) the location of the antinodes and; (3) the displacement at any point in the plate.

Nodes and antinodes are described in terms of deflection and slope respectively. With this in mind several existing optical systems capable of measuring deflections and slopes were investigated. With the exception of one study by Nickola (11) these had been applied only to static studies and it was hoped that they would be extended to include the dynamic case. These systems were all set up in the laboratory and evaluated and it was found that the shadow moiré method for deflection measurement and the Salet-Ikeda method for slope measurement yielded the best results. These were hence chosen for the study.

Three plate specimens were investigated; a cantilever beam, a square cantilever plate and a free circular plate. All were made of thin plexiglass.

For the analysis of nodes the shadow moiré system using a

high intensity light source was set up. The specimens were sprayed with flat white paint to give a matte finish. Upon adjusting the grid and exciting the plate it was found that highly definable nodal patterns were revealed. These patterns were recorded photographically. To locate the antinodes the Salet-Ikeda system was set up. This time the specimens were sprayed on the back surface so as to give a reflective front surface. By exciting the plate and using the camera as the pinhole partial antinodes in a particular direction were recorded. By superimposing the partial antinodes the true antinodes were revealed directly. Displacements were found by using the shadow moiré deflection method with a stroboscope as the light source. In this manner fringe motion could be "stopped" at any point in the vibration cycle and the displacement recorded photographically. As a means of evaluating the optical results theoretical solutions and sand patterns were offered for locating the nodes. Antinode locations were compared with theory.

II. CONCLUSIONS

From the investigation the following conclusions were drawn:

(1) Nodes may be located in any vibrating flat or nearly flat plate having an amplitude of vibration greater than .001".

(2) Antinodes may be located in any vibrating flat

or nearly flat plate having a minimum change in dynamic slope of .0002 rads. (typical)

(3) Dynamic displacements may be determined in any vibrating flat or nearly flat plate having an amplitude of vibration greater than .001".

III. SUGGESTIONS FOR FUTURE RESEARCH

Very little needs to be said regarding improvement of the actual equipment or arrangements used in the experiments. However, as it was pointed out in the last chapter a better means of inducing vibration is needed. Therefore it is recommended that an acoustical generator be used in the future.

The investigation undertaken in this thesis was limited to the study of flat plates under steady state conditions. Therefore two possible fields of further investigation are suggested: (1) the application of the technique to spherical and arbitrary surfaces and; (2) the study of transient conditions. It is anticipated that both these problems may be solved by slight modifications to the existing equipment. In order to "capture" the transient waves it is suggested that high speed photography be used. Since the shortest exposure time in this study, using ASA 3000 film, was 2 seconds it is apparent that a more intense light source will have to be found.

The second order fringes observed in most of the photo-

graphs are an interesting phenomenon. Since it is suspected that they are the moiré patterns of the two maximum amplitude fringe patterns it is wondered if the same effect could not be achieved with just one grid attached to the vibrating specimen. This is worthy of investigation.

The optical systems for the shadow moiré method and the Salet-Ikeda method are almost identical. It is therefore suggested that they be incorporated together in a vibration analysis instrument.

BIBLIOGRAPHY

1. Chladni, E. F., "Entdeckung in d. Theorie d. Klanges," 1787, only available information.

2. Waller, M. D., Chladni Figures, A Study in Symmetry, G. Bell and Sons Ltd., London, 1961.

3. Savart, M., "Sur la Communication des Mouvemens Vibratories entre les Corps Solides," Annales de Chimie, vol. 14, 1820, p.p. 113 - 167.

4. Faraday, M., "On a Peculiar Class of Acoustical Figures," Philisophical Transactions, 1831, p.p. 299 - 340.

5. Wood, A. B., A Textbook of Sound, G. Bell and Sons Ltd., London, 1946.

6. Dye, D. W., N.P.L. Reports, 1928.

7. Osterberg, H., "An Interferometer Method of Studying the Vibrations of an Oscillating Quartz Plate," Journal of the Optical Society of America, vol. 22, no. 19, 1932, p.p. 19 - 35.

8. Thornton, B. S. and Kelly, C. J., "Multiple-Beam Interferometric Method of Studying Small Vibrations," Journal of the Optical Society of America, vol. 46, no. 3, 1956, p.p. 191 - 194.

9. Powell, R. L. and Stetson, K. A., "Interferometric Vibration Analysis by Wavefront Reconstruction," Journal of the Optical Society of America, vol. 55, no. 12, 1965, p.p. 1593 - 1598.

10. Wasil, B. A., Merchant, D. C. and Del Vecchio, J. J., "Photogrammetric Measurements of Dynamic Displacements," Experimental Mechanics, vol. 5, no. 10, 1965, p.p. 332 - 339.

11. Nickola, W. E., "The Dynamic Response of Thin Membranes by the Moiré Method," paper presented at the spring meeting of the SESA, May, 1966.

12. Theocaris, P. S., "Moiré Fringes: A Powerful Measuring Device," Applied Mechanics Review, vol. 15, no. 5, 1962, p.p. 333 - 339.

13. Duncan, J. P., "The Optical Survey of Curved Surfaces," departmental paper, Dept. of Mechanical Engineering, University of British Columbia, 1966.

14. Weller, R. and Shepard, B. M., "Displacement Measurement by Mechanical Interferometry," Proceedings of the SESA, vol. 6, no. 1, 1948, p.p. 35 - 38.

15. Theocaris, P. S., "Moiré Method in Plates," Proceedings of the Colloquiam of the International Association of Shell Structures, Warsaw, 1963.

16. Theocaris, P. S., "Isopachic Patterns by the Moiré Method," Experimental Mechanics, vol. 4, no. 6, 1964, p.p. 153 - 159.

17. Ebbeni, J., "Observation en Incidence Oblique des Phenomenes de Moire par Reflexion sur une Plaque Gauchie," the Bulletin of the Royal Belgium Academy (Science Division), vol. 50, 1964, p.p. 114 - 124.

18. Middleton, E., "A Reflection Technique for the Survey of the Deflection of Flat Plates," paper presented at the Mechanical Engineering Dept., University of Sheffield, Jan. 1966.

19. Ligtenberg, F. K., "The Moiré Method - A New Experimental Method for the Determination of Moments in Small Slab Models," Proceedings of the SESA, vol. 12, p.p. 83 - 89, 1954.

20. Theocaris, P. S., "Moiré Patterns of Slope Contours in Flexed Plates," Experimental Mechanics, vol. 6, no. 4, 1966, p.p. 212 - 217.

21. Theocaris, P. S. and Koutsabessis, A., "Slope Measurement by means of Moiré Fringes," Journal of Scientific Instruments, vol. 42, 1965, p.p. 607 - 610.

22. Sabin, P. G., "Experimental Techniques for the Study of Elastic Flexure," M. Eng. thesis, University of Sheffield, 1964.

23. Duncan, J. P. and Brown, C. J. E., "Slope Contours in Flexed Elastic Plates by Salet-Ikeda Technique," Proceedings of the First International Congress on Experimental Mechanics, Pergamon Press, New York, 1963.

24. Young, D., "Vibration of Rectangular Plates by the Ritz Method," Journal of Applied Mechanics, vol. 17, 1950, p.p. 448 - 453.

25. Barton, M. V., "Vibration of Rectangular and Skew Cantilever Plates," Journal of Applied Mechanics, vol. 18, 1951, p.p. 129 - 134.

26. Harris, C. M. and Crede, C. E., Shock and Vibration Handbook, vol. 1, McGraw-Hill Book Co., 1961.

27. Post, D., "Sharpening and Multiplication of Moiré Fringes," paper presented at the Mechanical Engineering Dept., University of Sheffield, Jan. 1966.

28. Young, D. and Felgar, R. P., "Tables of Characteristic Functions Representing Normal Modes of Vibration of A Beam," Bulletin of the University of Texas, 1949.

APPENDIX A

BEAM AND PLATE EQUATIONS

Cantilever Beam

A very complete set of tables of the characteristic functions of a vibrating beam is given by D. Young and R. P. Felgar (28). These values were calculated using the Ritz method and vary from the exact method by no more than 1.5% which is quite adequate for this study. The following values were hence taken from these tables.

The natural frequency of the nth mode is given by:

$$f_n = \frac{\beta_n^2}{2\pi}\sqrt{\frac{EI}{\mu}}$$

where $\beta_n L$ is tabulated below in Table 2.

n	$\beta_n L$
1	1.875
2	4.694
3	7.855
4	10.996
5	14.137

TABLE 2

For any particular mode n the deflection is given by:

$$w_n = A\Phi_n$$

Where A is the amplitude coefficient and Φ_n the characteristic function that must satisfy the required boundary conditions. Similarly for slope:

$$w_n' = A\Phi_n'$$

Obviously the nodes and antinodes may be readily determined by equating w and w' to zero respectively. Thus for a node:

$$\Phi_n = 0$$

and for an antinode,

$$\Phi_n' = 0$$

In the reference tables, values for Φ_n and Φ_n' are tabulated in increments of 1/50 of the beam length and hence to find the zero values a certain amount of interpolation is involved. Table 3 shows the relative positions of the nodes and antinodes as a ratio of x/L . These may be compared to values given in the Shock and Vibration Handbook (26) on page 7 - 14.

Square Cantilever Plate

From Young's paper (24) the natural frequency is seen to be given by:

$$f_n = \frac{\beta_n}{2\pi a^2}\sqrt{\frac{D}{\rho t}}$$

where β_n is given in Table 4.

Circular Free Plate

The natural frequency of a circular free plate is given on page 1-15 of the Shock and Vibration Handbook (26) and is:

$$f_n = \frac{\beta_n}{2\pi a^2}\sqrt{\frac{Et^2}{\rho(1-\nu^2)}}$$

where β_n is given in Table 5.

MODE	LOCATION OF NODES (N) AND ANTINODES (A) IN A VIBRATING BEAM
1	
2	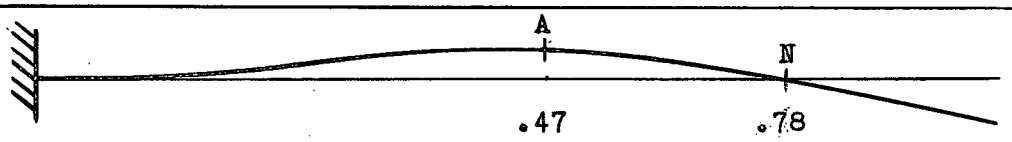
3	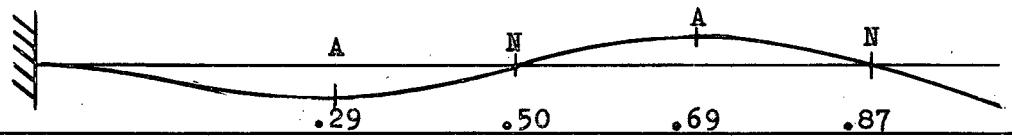
4	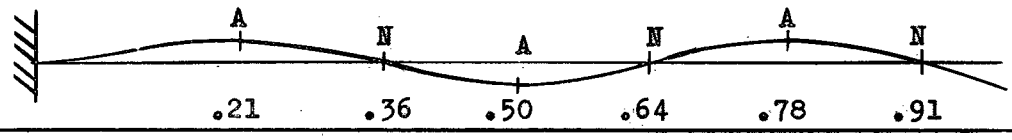
5	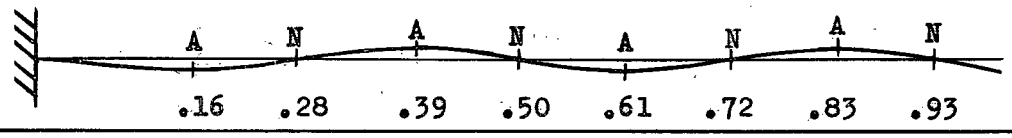

TABLE 3

n	β_n
1	3.494
2	8.547
3	21.44
4	27.46
5	31.17

TABLE 4

n	β_n
1	6.09
2	10.53
3	14.19
4	23.80
5	40.88
6	44.68
7	61.38
8	69.44

TABLE 5